



# Spatial organization of gold and alteration mineralogy in hydrothermal systems: wavelet analysis of drillcore from Sunrise Dam Gold Mine, Western Australia

MARK A. MUNRO<sup>1,2\*</sup>, ALISON ORD<sup>1,3</sup> & BRUCE E. HOBBS<sup>1,4</sup>

<sup>1</sup>*Centre for Exploration Targeting, University of Western Australia, WA 6009, Australia*

<sup>2</sup>*Present address: Geological Survey of Western Australia, Department of Mines, Industry Regulation and Safety, Mineral House, 100 Plain Street, East Perth WA 6004, Australia*

<sup>3</sup>*School of Resources and Environmental Engineering, Hefei University of Technology, Hefei 230009, China*

<sup>4</sup>*CSIRO, Perth, WA 6102, Australia*

\*Correspondence: [mark@munrogeoscience.com](mailto:mark@munrogeoscience.com)

**Abstract:** The spatial distributions of mineralization and alteration in hydrothermal systems are complex and are often considered to be cryptic and problematic to quantify. We used wavelet analysis of conventional hyperspectral drillcore logs to demonstrate quantitatively that primary Au mineralization, common vein-hosted mineralogy (calcite and ankerite), host rock alteration mineralogy (sericite and chlorite) and regional-scale metamorphic assemblages (amphibole) organize spatially as multifractals. This documentation of multifractal spatial organization in Au and alteration mineralogy is sufficient to show that they are the result of underlying deterministic dynamic processes as opposed to random stochastic processes. The application of wavelets to three ore bodies (GQ, Vogue and Cosmo East) from the highly endowed Archaean Sunrise Dam hydrothermal Au system of Western Australia shows that the spatial organizations of Au and ankerite are more closely associated in GQ than in Vogue. The spatial organization of Au in Vogue is more strongly associated with calcite. Primary Au mineralization and infill carbonate mineralogy are more complexly organized than sericitic and chloritic host rock alteration. Although demonstrated here for a hydrothermal system, wavelet analysis is readily applicable to downhole or outcrop data from any deposit type.

A range of factors conspires to control the location of hydrothermal alteration and Au mineralization in the Earth's crust. These include the micro- to lithospheric-scale structure, fluid availability, fluid composition (including pH), pressure–temperature conditions, the distribution of primary rock types and the length scales of fluid–rock interactions. As a consequence of the interconnected nature of these factors, the spatial organization of mineralization and alteration in hydrothermal systems is complex (e.g. Fig. 1) and is often considered cryptic and problematic to quantify. This recognition that ore deposits, such as hydrothermal systems, are the small-scale products resulting from a range of lithospheric processes supports a shift in focus from conventional deposit-scale study to a holistic, multi-scale, mineral systems approach to examine and interpret hydrothermal systems (Wyborn *et al.* 1994; Hobbs *et al.* 2000; Ord *et al.* 2012; McCuaig & Hronsky 2014; Vearncombe & Zelic 2015; Occhipinti *et al.* 2016; Wyman *et al.* 2016).

Another paradigm for the formation of hydrothermal systems is that they operate as open flow

chemical reactors held far from equilibrium throughout their evolution and that they exhibit non-linear behaviour (Lester *et al.* 2012; Ord *et al.* 2012, 2016). This is achieved via the constant introduction of heat and fluids carrying diverse chemical species, during which there is potential for mineralization (Ord *et al.* 2012). A fundamental characteristic of systems operating under non-linear conditions is that they should develop organized spatial patterns as a result of the non-linear interactions between the processes occurring during their evolution (e.g. Beck & Schlogl 1993; Bak 1996; Chainais 2006; Sornette 2006) – that is, their spatial organizations should be fractal. A fractal signal is one that shows a repetition of geometric components, or patterns, when examined over a range of observation scales (Mandelbrot 1982; Feder 1988; Schroeder 1991). These are not necessarily exact replications, but are statistically self-similar. The scaling behaviour of geometric repetitions is quantified by a scaling law exponent (the fractal dimension, or  $D$ ). Simple fractals (monofractals) have only one fractal dimension, but natural systems are often more

From: GESSNER, K., BLENKINSOP, T. G. & SORJONEN-WARD, P. (eds) *Characterization of Ore-Forming Systems from Geological, Geochemical and Geophysical Studies*. Geological Society, London, Special Publications, **453**, <https://doi.org/10.1144/SP453.10>

© 2018 The Author(s). Published by The Geological Society of London. All rights reserved.

For permissions: <http://www.geolsoc.org.uk/permissions>. Publishing disclaimer: [www.geolsoc.org.uk/pub\\_ethics](http://www.geolsoc.org.uk/pub_ethics)

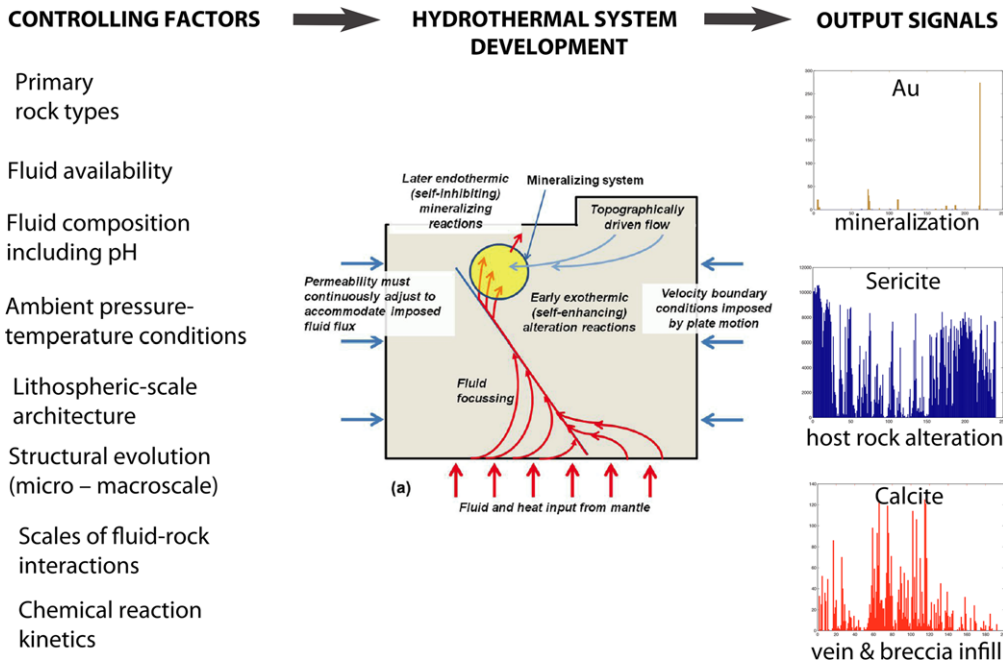


**Fig. 1.** The geometry of hydrothermal mineral systems, the factors contributing to their development and examples of the signals they produce. System development is driven by the interaction of mantle-derived and topographically driven fluids. Downhole mapping of mineral phase abundance and composition (right) is provided by hyperspectral reflectance imaging. Hydrothermal system geometry modified from Ord *et al.* (2016).

complex and may be composed of multiple geometric components that each have different fractal dimensions (i.e. they are multifractal) (Arneodo *et al.* 2002). These fractal spatial organizations are the hallmark of non-linear processes. Therefore, if hydrothermal mineralizing systems do indeed operate as non-linear systems, then they should display multifractal spatial organizations that can be identified and quantified from the signals extracted from the system.

Drillcores allow direct and detailed mapping of the spatial distributions of primary mineralization and alteration assemblages in hydrothermal systems and the relationships between them. The observations and signals extracted from drillcore are integrated with a range of multi-scale approaches, including remote sensing (Pour *et al.* 2013), field- and pit-based geological mapping (e.g. Sanislav *et al.* 2016) and numerical modelling (e.g. Haynes *et al.* 1995; McLellan *et al.* 2007; Ingebritsen *et al.* 2010) to develop an understanding of the system's development in space and time. Methods of interrogating drillcore include lithological and structural logs, Au, multi-element and isotopic analysis, and hyperspectral reflectance imaging (e.g. Roache *et al.* 2010; Wang *et al.* 2017). Of these methods, hyperspectral reflectance imaging

represents an efficient, non-destructive and cost-effective means of furnishing comprehensive digital profiles of mineral abundance and/or composition as drillcore becomes available. Therefore the technique is now routinely applied to the examination of hydrothermal Au systems (e.g. Cudahy *et al.* 2009; Tappert *et al.* 2013), in addition to a range of other deposit types, including Fe ore (Ramananidou *et al.* 2015), volcanic-hosted massive sulphide ores (Jones *et al.* 2005; Duuring *et al.* 2016), porphyry Cu (Zadeh *et al.* 2014) and regolith characterization (Laukamp *et al.* 2016). The interpretation and comparison of different hyperspectral datasets is commonly carried out using qualitative visual comparisons or through empirical and/or statistical measures. However, one-dimensional series of concentrations, such as hyperspectral mineral abundances or Au assays, are ideal formats for the quantitative application of techniques designed to test for the presence of multifractal spatial organizations and therefore for non-linear behaviour in the underlying processes operating during the system's evolution.

Interrogation for the presence of multifractal spatial organization in one-dimensional signals, such as those derived from drillcore, can be carried out using wavelet-based analysis (Arneodo *et al.*

## QUANTIFYING HYDROTHERMAL SYSTEMS

1995, 2002). This method is well-established and is objective, readily accessible and rapid to implement. The procedure involves taking a wavelet (a localized oscillating waveform) and scanning different sizes of it incrementally across a dataset, returning a measure of the local signal behaviour at a range of length scales. By evaluating for patterns of self-similarity in different geometric components of the signal across this range of length scales, wavelet analysis provides a quantification of the scaling law exponents (fractal dimensions) that are present.

Wavelet-based analysis was applied to a large, well-endowed hydrothermal system (the late Archaean Sunrise Dam Gold Mine of Western Australia) to address quantitatively three important questions:

- (1) Do hydrothermal systems organize spatially as multifractals, i.e. do they record evidence for non-linear underlying processes?
- (2) If so, can variations in the spatial organization of Au and mineral phases be identified within the system using these multifractal signatures?

- (3) Can a comparison of the multifractal signatures of Au and different mineral phases be used to determine whether they are genetically associated with one another?

The Sunrise Dam Gold Mine (Figs 2 & 3) was selected because of the availability of spatially referenced Au assay and hyperspectral reflectance datasets from large numbers of drillcores intersecting three texturally and structurally distinct ore bodies: GQ, Vogue and Cosmo East. The analysis was applied to 0.5 m resolution downhole concentration datasets for primary mineralization (Au), vein and breccia cement-forming carbonates (calcite and ankerite), host rock alteration associated with mineralization (sericite) and mineralogy involved in host rock alteration processes not directly related to the mineralization (chlorite and amphibole). This study builds on the foundation laid by Ord *et al.* (2016), which presented a detailed overview of wavelet analysis and a few key demonstrations of the method applied to Au, sericite and chlorite. Wavelet analysis is complemented by the determination of Hurst exponents (Feder 1988; Arneodo *et al.* 2003; Sprott 2003) to

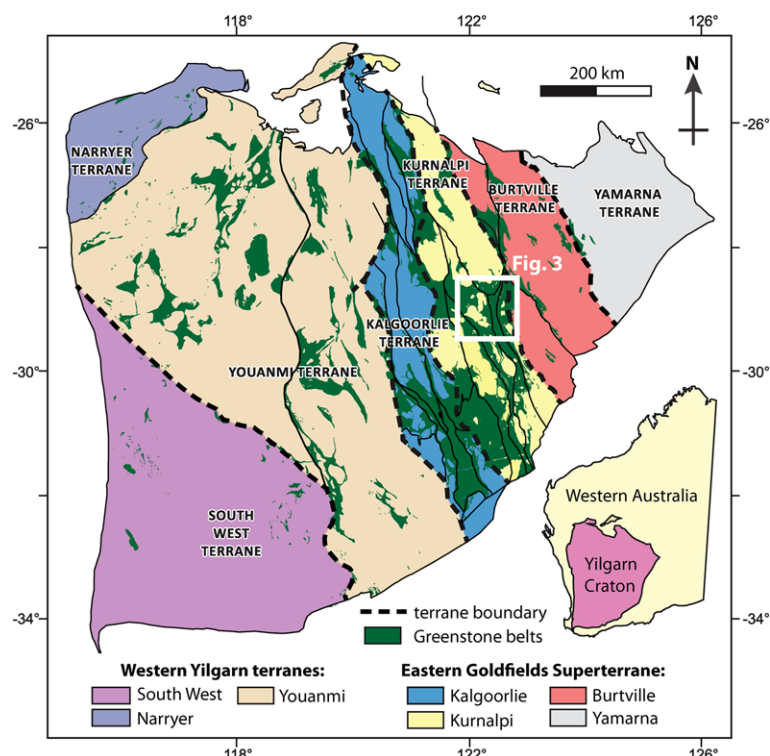


**Fig. 2.** Map of the Archaean Yilgarn Craton of Western Australia showing the major terranes and the distribution of greenstone belts across the craton. The late Archaean Sunrise Dam Gold Mine is located in the Kurnalpi terrane, within the box (the area of Fig. 3). Modified from Hollis *et al.* (2015).

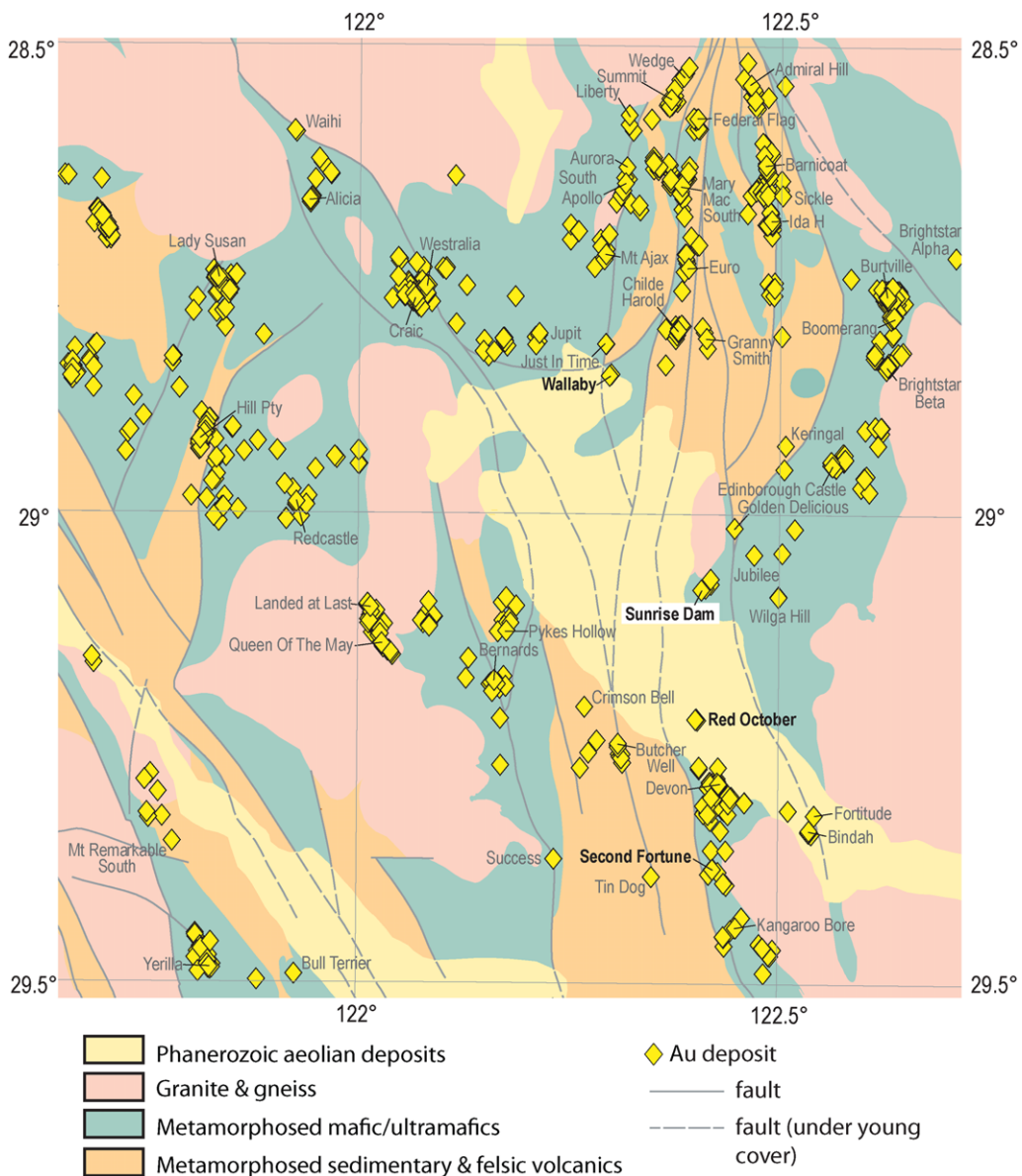


**Fig. 3.** Interpreted bedrock geology map (1:2 500 000 scale) of part of the Kurnalpi terrane around the Sunrise Dam Gold Mine. Yellow diamonds mark the locations of Au deposits in the area. Some key larger deposits and closed mines are labelled in standard text; bold black text indicates mines that are either currently operating or under development (January 2017), including Sunrise Dam. Modified from Cooper *et al.* (2017).

investigate the absolute length scales of long-range correlation in key examples of the Au and mineral phases examined. Although the wavelet technique was applied here to 0.5 m resolution Au assay and mineral abundance data from a model hydrothermal system, it is equally applicable to down-hole datasets of any resolution and from any deposit type.

### Archaeon Sunrise Dam hydrothermal system

#### *Geological setting, Au mineralization history and structural evolution*

The Late Archaeon Sunrise Dam Au deposit (Figs 2 & 3) is situated in the Laverton tectonic zone of

## QUANTIFYING HYDROTHERMAL SYSTEMS

the Kurnalpi terrane in the Archaean Yilgarn Craton, Western Australia. The deposit is hosted by volcanoclastic rocks (basaltic to andesitic) and banded iron formations (magnetite-rich shales and turbidites) (Baker *et al.* 2010). These country rocks have been intruded by a series of sills and dykes, primarily quartz–feldspar porphyries, but locally lamprophyres and ultramafic rocks. Brown *et al.* (2002) conducted U–Pb zircon dating of pre-mineralization porphyry dykes, Ar/Ar dating of fuchsite formed in the Sunrise shear zone, Re–Os dating of vein-hosted molybdenite and U–Pb dating of xenotime and monazite interpreted to be syn-mineralization. The interpretation of these data and their uncertainties have been the subject of discussion (Brown *et al.* 2002; Mueller 2002; Blenkinsop *et al.* 2007) and the age of mineralization has been suggested to be *c.* 2670 Ma (Baker *et al.* 2010) and between 2665 and 2650 Ma (Yardley & Cleverley 2015). The peak metamorphic conditions are greenschist facies, reflected by both the regional metamorphic paragenesis and localized alteration assemblages; however, the timing of Au and sulphide mineralization relative to peak metamorphism remains unconstrained (Baker *et al.* 2010). The extensive Sunrise Dam system is subdivided into several structurally and petrologically distinct ore bodies of differing size and grade (Fig. 4).

Blenkinsop *et al.* (2007) and Baker *et al.* (2010) identified a seven-stage structural evolution at Sunrise Dam, building on a previous framework established by Miller & Nugus (2006). Throughout this deformation chronology, weak Au mineralization (*c.* 0.25–1.5 g t<sup>-1</sup>) accompanied D<sub>1</sub>, with stronger mineralization associated with D<sub>3</sub>, D<sub>4a</sub> and D<sub>4b</sub> (averaging grades of 2.8, 16.5 and 4.25–18 g t<sup>-1</sup>, respectively). Using this deformation framework and mineralization history, a four-group classification scheme was proposed for the Au lodes (Blenkinsop *et al.* 2007; Baker *et al.* 2010) based principally on their dominant hosting structures. A summary of structure, alteration and mineralization in each of the four groups is presented here.

Group I ore bodies are hosted primarily within gently to moderately (*c.* 20–40°) NW-dipping shear zones (the GQ, Mako, Sunrise, Midway and Cleo). The shear zones are dominantly ductile, characterized by strong S–C fabric development, and have local subparallel laminated veins and breccia veins. The Sunrise shear zone is the largest structure within the Sunrise Dam Gold Mine, marked by a zone of intense shear-related sericite foliations up to 40 m wide (Blenkinsop *et al.* 2007). Other shear zones in the group form a series of typically metre-wide high strain zones that dip *c.* 10–15° steeper than the larger Sunrise shear zone. Au mineralization is hosted within quartz–carbonate ± pyrite ± arsenopyrite veins within an intense penetrative

chlorite–sericite D<sub>3</sub> fabric. Associated wall rock alteration consists of the assemblage quartz–sericite–carbonate–pyrite–chlorite. Mineralization in Group I is also hosted in younger laminated quartz–carbonate veins that cross-cut syn-D<sub>3</sub> veining (interpreted as syn-D<sub>4</sub>).

Group II ore bodies are dominantly breccia- and vein-hosted, situated within steeply dipping D<sub>3</sub> shear zones, such as the Summercloud, Watu and Predator. Mineralization is also (less frequently) contained within penetrative fabrics. Localized zones of brecciation may be up to several metres wide, consisting of angular sericite-replaced fragments of volcanic units encased within quartz–carbonate cements. Veining (often steeply dipping) may be up to 5 m in width, composed of carbonate–pyrite–arsenopyrite–quartz. Other gently NW-dipping veins containing Au, tellurides and As sulphides have been interpreted as syn-D<sub>4</sub>, contemporaneous with dextral normal faulting.

Group III type ore bodies (e.g. the Cosmo and Dolly lodes) are hosted within zones of stockwork veins and brecciation up to 20 m across. Stockwork veining contains carbonate–chlorite–quartz ± sericite ± pyrite ± arsenopyrite, associated with sericite–quartz–pyrite–ankerite ± arsenopyrite alteration of the surrounding volcanic host rocks. Breccia clasts are cemented by quartz and carbonate. Group III ore bodies are primarily associated with the D<sub>4a</sub> deformation, characterized by NE–SW directed bulk shortening and dextral fault kinematics.

Group IV ore bodies encompass those hosted within the extensively sericite-altered Dolly quartz–feldspar porphyry, where mineralization is contained within narrow, steep, As-rich veining.

Within this previously determined classification of the ore bodies, the GQ ore body analysed in this study constitutes part of Group I, those hosted in gently to moderately northwesterly dipping shear zones. The Vogue ore body has been interpreted to have a similar history to GQ (Group I), but also experienced a later event (probably remobilization), which locally enhanced Au grades (Roache, pers. comm., 2017). Cosmo East forms part of the Group III stockwork vein and breccia lodes.

### Mineral distribution framework: alteration assemblages and vein-/breccia-forming mineralogy

Chlorite is abundant (e.g. Fig. 5a) and often forms penetrative schistosities in many of the host rocks, in addition to intense S–C fabrics in the prominent shear zones that characterize the system. Although constituting a minor component of veining and hydrothermal alteration assemblages (Blenkinsop

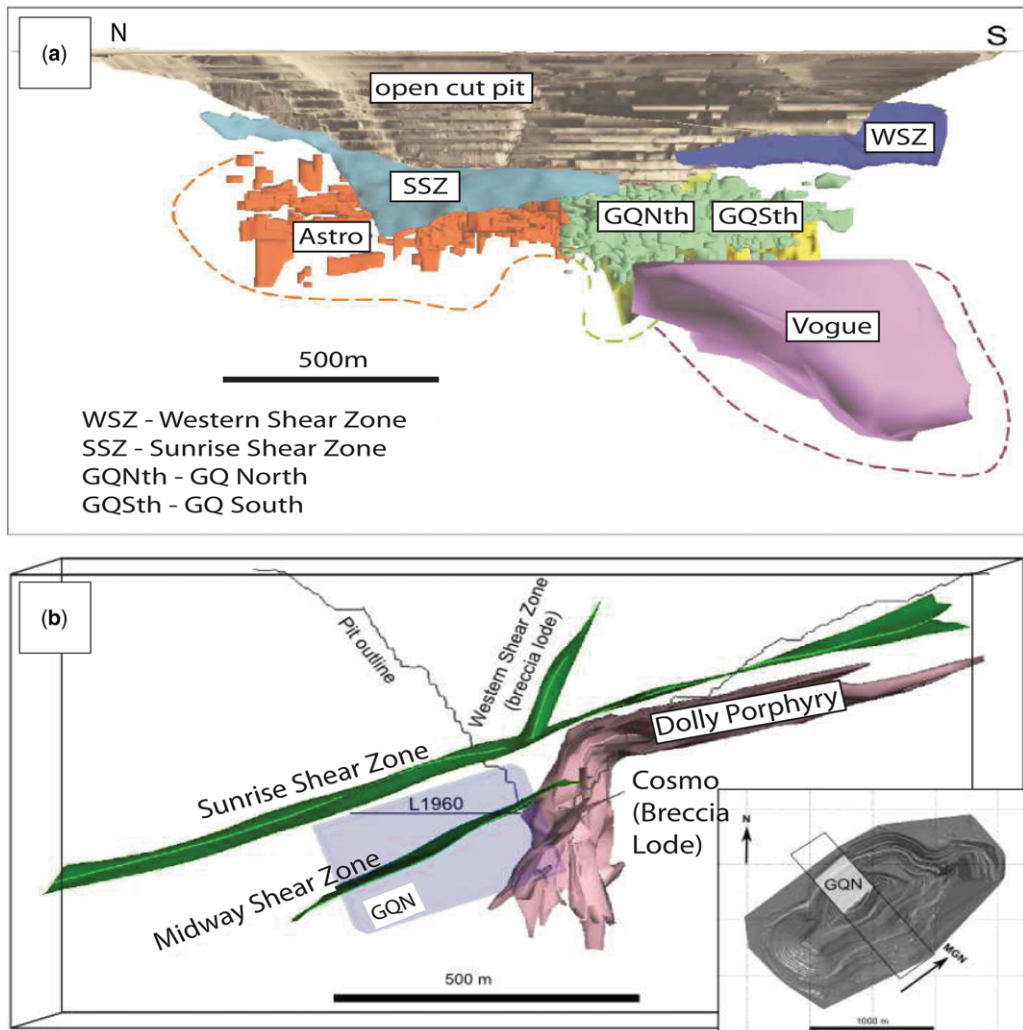


**Fig. 4.** (a) North–south (mine grid) cross-section of three-dimensional model of the ore bodies at Sunrise Dam showing their relationship to the mine pit. (b) Vertical NW–SE-striking cross-section view of a three-dimensional model of Sunrise Dam showing the Cosmo breccia lode and its relationship to the Dolly porphyry, prominent shear zones and GQ North. The inset in (b) shows the position of the NW–SE cross-section in plan view relative to true north (N) and mine grid north (MGN). Drillcore from Vogue, GQ (North and South) and Cosmo East were used in this study. Modified from Hill *et al.* (2014).

*et al.* 2007), textural and compositional investigations have not regarded chlorite to be a major component of proximal alteration assemblages directly related to Au mineralization (e.g. Blenkinsop *et al.* 2007; Baker *et al.* 2010; Yardley & Cleverley 2015). Instead, chlorite has been noted as becoming locally more dominant away from alteration zones (e.g. Blenkinsop *et al.* 2007). Chlorite–calcite assemblages at Sunrise Dam have been largely regarded as an early alteration not associated with mineralization (Roache, pers. comm., 2017).

Therefore the concentration and distribution of chlorite in the Sunrise Dam system appears to dominantly reflect host rock alteration not directly associated with the primary mineralization.

Alteration of the host rocks in selvages proximal to mineralization and fluid conduits (veining, brecciation and shear zones) is dominantly sericitic (Blenkinsop *et al.* 2007; Yardley & Cleverley 2015). The sericite composition ranges from paragonite and muscovite (Al-rich) to phengite (Mg-bearing). Investigations of Sunrise Dam conducted

## QUANTIFYING HYDROTHERMAL SYSTEMS

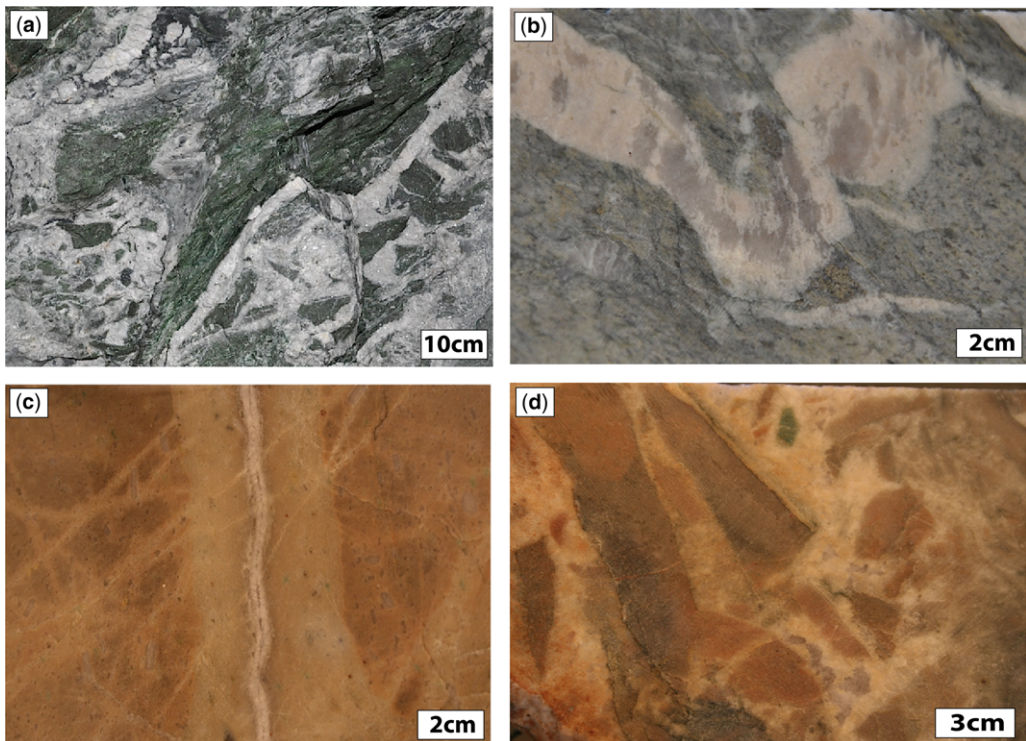


**Fig. 5** (a) Breccia zone with basalt host rock clasts encased in calcite and quartz cement. Basalt clasts have been extensively replaced by chlorite during host rock alteration. (b) Folded ankerite–quartz veining in strongly sericite-metasomatized andesite from GQ. Sericite in this section is dominantly paragonite and muscovite; visible pyrite is locally associated with the veining. (c) Calcite  $\pm$  ankerite  $\pm$  quartz veining in quartz–feldspar porphyry from Cosmo East. Phenocrysts are dominantly quartz. Feldspar in the groundmass of the host rock surrounding the veins has been locally replaced by sericite. Chlorite is present in minor abundance. (d) Brecciation of a similar quartz–feldspar porphyry host rock from Cosmo East. Angular clasts are encased in calcite  $\pm$  ankerite  $\pm$  quartz cement.

by AngloGold Ashanti have demonstrated a spatial correlation between paragonite and muscovite-forming reactions and Au mineralization in GQ. Conversely, phengite-dominated zones correspond to those that are barren or poorly mineralized. Although sericite dominates, carbonates (calcite and dolomite to ankerite) and (minor) chlorite also participate in host rock alteration associated with mineralization. Carbonate wall rock alteration intensifies away from the mineralization zones in some of the Group I ore bodies.

Dominant vein and breccia cement-forming phases associated with mineralization are calcite, ankerite to dolomite, and quartz (e.g. Fig. 5b–d) (Blenkinsop *et al.* 2007). Individual veins are either composed exclusively of one of these phases, or a combination. Where quartz-only and carbonate-only veins coexist, they may display local overprinting at the mesoscale, but display mutual cross-cutting relationships at the ore body scale (Hantler

2009; Hill *et al.* 2014). Sericite and chlorite may also be present in veining, but are less abundant.

Structural and petrological investigations suggest that carbonate-forming processes at Sunrise Dam (calcite and ankerite to dolomite) are entirely secondary – associated with vein and brecciation infill, and host rock alteration. The protoliths that host the deposit (basaltic to andesitic volcanic and volcanioclastic rocks, and banded iron formations) lack primary carbonates. Accordingly, calcite and ankerite distributions in the system are primarily structurally controlled (dependent on the scales of deformation partitioning, the spatial volumes of veining and the fluid composition, including pH).

Amphibole is another common phase throughout Sunrise Dam. Petrological investigations of the alteration (e.g. Blenkinsop *et al.* 2007; Baker *et al.* 2010; Yardley & Cleverley 2015) have not interpreted amphibole to be part of the alteration

assemblages spatially associated with mineralization. However, very minor amounts may be vein-hosted (Roache, pers. comm., 2017). Amphibole abundances within Sunrise Dam are instead interpreted to reflect protolith distribution – with moderate to high abundances corresponding to andesite, basalt and ultramafic protoliths. Amphibole in these rock types has been interpreted as both primary and a product of regional metamorphism.

## Methods

### *Hyperspectral infrared reflectance spectroscopy*

Hyperspectral reflectance analysis now plays an integral part in determining spatial distributions in the abundance, and composition, of key mineral phases in a range of ore deposits (e.g. Cudahy *et al.* 2009; Roache *et al.* 2010; Tappert *et al.* 2013; Wang *et al.* 2017). Incident electromagnetic energy is applied to a rock volume, with reflectance measured as a ratio between the transmitted energy and that reflected by the surfaces of the mineral phases. The wavelengths of electromagnetic energy relevant to hydrothermal systems are those in the visible to near-infrared and short-wave infrared (SWIR) ranges (0.4–1.4 and 1.4–3 µm, respectively). The reflection response of key alteration phases, such as sericite and chlorite, are dependent on the cation–hydroxyl group configurations in their lattices (Cudahy *et al.* 2009; Wang *et al.* 2017). Hydroxyl groups bonded to specific cations (e.g. Mg<sup>2+</sup>, Al<sup>3+</sup> and Fe<sup>2+</sup>) vibrate under exposure to specific wavelengths of electromagnetic energy, producing diagnostic absorption features that may be used to discriminate between mineral phases. Wavelength-specific absorption features under SWIR are present in paragonite (2190 nm), muscovite (2200 nm) and phengite (2220 nm) compositional members (Blenkinsop *et al.* 2007). These absorption features have been used to map the distributions of mineral phases such as sericite and chlorite at Sunrise Dam, and also compositional variations within them (Blenkinsop *et al.* 2007).

The SWIR reflectance can also discriminate between calcite ( $\text{CaCO}_3$ ) and ankerite–dolomite series carbonates bearing additional cations ( $\text{Fe}^{2+}$ ,  $\text{Mg}^{2+}$  and  $\text{Mn}^{2+}$ ). Calcite has a higher wavelength absorption feature (typically 2335 nm) than ankerite and dolomite (2325 and 2320 nm, respectively). However, confident discrimination between the  $\text{CaFe}(\text{CO}_3)_2$  (ankerite) and  $\text{CaMg}(\text{CO}_3)_2$  (dolomite) series end-members under hyperspectral reflectance is problematic because of their similar wavelengths. Therefore, following previous investigations of the Sunrise Dam deposit, the term ‘ankerite’ is used

here throughout to encompass all phases in the ankerite–dolomite series.

Hyperspectral images of drillcore are subdivided into pixels, typically of the order of a couple millimetres to a few centimetres, each interrogated across a range of wavelengths spanning the visible to near-infrared and SWIR to evaluate the presence or absence of individual mineral phases. Modern hyperspectral imaging techniques now allow analytical resolution down to scales of the order of 100s of micrometres. The acquired pixel data may be used either to quantify the downhole concentrations of each mineral phase, or to map the downhole variations in compositional end-members. Recent investigations have successfully utilized SWIR absorption features to map the distributions of sericite (white mica) composition at Sunrise Dam and the Kanowna Belle gold deposit (Wang *et al.* 2017), also situated in the Eastern Goldfields Superterrane. In the GQ ore body at Sunrise Dam, SWIR absorption features have demonstrated that zones of paragonite- and muscovite-forming reactions spatially correspond with Au precipitation; phengite-forming reactions dominate within barren host rock (Fig. 6).

### *Sunrise Dam drillcore data acquisition*

This study used 207 independent drillcores: 117 drillcores from the GQ ore body, 64 from Vogue and 26 from Cosmo East. Most drillcores from GQ range from 135 to 300 m in length (90%), with some extending between 300 and c. 508 m (10%). Most drillcores from Vogue range from 275 to 520 m in length (85%), with some extending between 560 and 1069 m (15%). Drillcores from Cosmo East range between 366 and 642 m in length. Table 1 presents the summary statistics for the data presented in the study. All intervals analysed represent fresh rock; they are therefore representative of the primary (hypogene) sections of the system and are unaffected by near-surface remobilization processes associated with oxidation and interaction with meteoric fluids.

Downhole sericite, chlorite, calcite, ankerite and amphibole abundance data for each hole were provided by AngloGold Ashanti. The sericite abundance is an aggregate of all compositions, incorporating paragonite, muscovite and phengite. All spectra and mineral abundances used in this study were generated using the same procedure. The abundances were derived from previously conducted hyperspectral reflectance spectroscopy campaigns of the drillcore from the three ore bodies. A SpecIm sisuROCK hyperspectral scanner was used to scan the core over the wavelength range 1000–2500 nm. A polystyrene standard with a known spectral response was analysed to calibrate the

## QUANTIFYING HYDROTHERMAL SYSTEMS

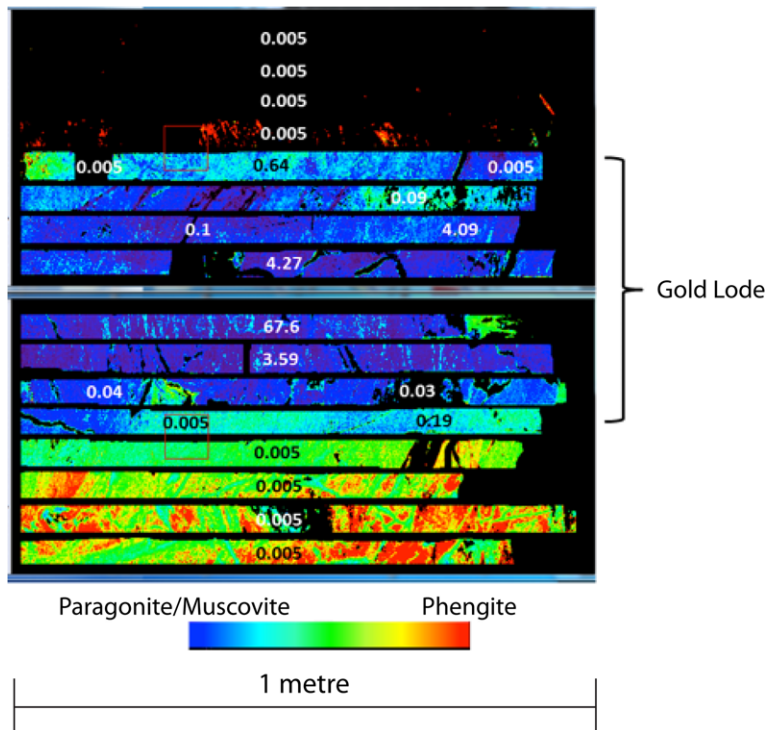


**Fig. 6.** Hyperspectral reflectance image of a 16 m span of drillcore from the GQ ore body showing how sericite (white mica) composition may be mapped. Blue (lower wavelength) end-members are paragonite and muscovite; red end-members are phengite; black represents an absence of sericite. Local Au grades (ppm) are indicated on the core. Paragonite- and muscovite-forming reactions correlate with the Au mineralized zone; phengite, or an absence of sericite, correlate with barren zones. Image provided by T. Roache, AngloGold Ashanti.

scanner. The core was scanned using a pixel resolution of  $1.6 \times 1.6$  mm. Following acquisition, the spectral data were initially processed to reflectance and then left as full wavelength reflectance spectra. They were also normalized to the hull of the reflectance spectrum between 1300 and 2450 nm (the range most relevant to the hydrous silicates and carbonates of interest).

Hyperspectral data are typically acquired at high resolutions of the order of c. 1–10 mm (1.6 mm in this study). However, Au assay data are routinely acquired at lower resolutions of the order of 0.5–1 m (0.5 m in this study). Therefore, to allow direct comparison with Au dynamics, the initial 1.6 mm resolution hyperspectral mineral concentration data were composited into 0.5 m concentration intervals corresponding with the 0.5 m Au assay intervals. Au and all mineral phases were analysed over the same interval within each individual drillcore. The entire length of each individual drillhole was utilized during wavelet analysis to maximize the amount of data used to produce the singularity spectra.

#### Wavelet analysis: theory and application to Sunrise Dam drillcore

**Fractals and multifractals.** Fractals are geometric patterns that show a repetition of geometric elements over a range of observation scales. This repetition is not necessarily exact, but is a statistical self-similarity. The behaviour of these repetitions with varying scale is quantified by an exponent of the scaling law; the fractal dimension,  $D$ , of the system. The suggestion of a fractal distribution for crustal ore deposits was initially put forward by Mandelbrot (1982) and later tested by Carlson (1991). The concept has since been applied worldwide to characterize deposit size and distribution (Blenkinsop 1994; Agterberg 1995; Ford & Blenkinsop 2008; Sun & Liu 2014; Ord *et al.* 2016), mineral prospectivity (Cheng 2007; Carranza 2009; Wang *et al.* 2012; Yuan *et al.* 2015), ore resource estimation (Wang *et al.* 2010) and assessment of the relationship between ore grade and tonnage (Turcotte 1986).

Multifractals are signals in which multiple sub-signals, or components, can be identified that behave

**Table 1.** Summary of drillcore statistics for the data presented in this study

	No. of drill cores	Total length (m)	Mean length (m)	Standard deviation (m)	Minimum length (m)	Maximum length (m)
<i>GQ</i>						
Au	102	23 025.0	227.97	71.56	135	508
Sericite	88	20 496.5	230.30	73.94	135	508
Chlorite	97	21 902.0	225.79	70.26	135	508
Calcite	98	22 860.0	233.27	71.03	135	508
Ankerite	101	23 356.0	231.25	71.77	135	508
Amphibole	82	18 854.0	229.93	68.87	135	508
<i>Vogue</i>						
Au	54	24 193.5	448.03	133.65	275	1069
Sericite	61	27 761.5	455.11	151.83	275	1069
Chlorite	62	27 764.0	455.15	151.44	275	1069
Calcite	57	26 130.0	458.42	144.47	275	1069
Ankerite	64	29 225.5	456.65	148.41	275	1069
Amphibole	41	19 748.0	481.66	169.36	275	1069
<i>Cosmo</i>						
Au	19	9212.0	484.84	84.25	366	642
Sericite	25	12 053.0	482.12	83.58	366	642
Chlorite	24	11 540.0	480.83	84.93	366	642
Calcite	25	12 066.0	482.64	83.72	366	642
Ankerite	18	8792.0	488.44	80.11	366	642

differently with varying scale (i.e. they have their own fractal dimensions). These sub-signals amalgamate to form a tiered hierarchical organization in frequency and in wavelength (spatial scale) of correlations. This hierarchical organization involves the replication of geometric features over a wide range of scales, with the greatest number of occurrences commonly at smaller observation scales, declining to fewer occurrences at larger observation scales.

*Wavelet transform modulus maxima method of wavelet analysis.* Analysing the properties of a multifractal signal can be carried out via a number of methods, the most widely used being the wavelet transform modulus maxima (WTMM) method (Arneodo *et al.* 1995). The WTMM method involves incrementally scanning a wavelet (a small signal packet) across the dataset multiple times, progressively varying its scale. The application of a wavelet in this manner is similar to the application of a box in the traditional box-counting method of fractal examination. The scale of a wavelet is expressed in octaves, with each octave subdivided into voices (Kumar & Foufoula-Georgiou 1997; Audit 2008). Wavelet size increases by a factor of two with each successive octave. This is analogous to Western musical notation, in which the audio frequency doubles with each octave. The number of octaves used controls the range of scales analysed; the number of voices used controls the number of scale increments analysed within this range. A mathematical definition and detailed discussion of octaves

and voices is available in Appendix B of Ord *et al.* (2016). The hypothetical signal shown in Figure 7 demonstrates how this multi-scale examination can be used to identify self-similarity at a range of scales within the master signal.

The maximum size of wavelet that may be applied to a signal (i.e. the maximum length scale of analysis, in octaves) is pre-determined by the number of data points (its length). The greater the length of a drillcore interval, the greater the range in wavelet scale that may be applied. Optimum singularity spectrum results are obtained when utilizing octave values close to, or at, the maximum range allowed. Using too narrow a range in octaves results in a malformed singularity spectrum due to the dataset being analysed over an inadequate range of length scales to evaluate the organizational (multifractal) hierarchy of the system. Importantly, for any singularity spectra to be straightforwardly compared, they must be derived from analyses utilizing the same wavelet parameters (configuration of octaves and voices).

The aim of the WTMM method is to decompose the master signal into the component fractals present within it. Monofractals are relatively simple signals and are fully quantified by a single scaling exponent, or  $D$ . However, multifractal systems are more complex and require quantification by a continuous spectrum of scaling exponents: a singularity spectrum (e.g. Fig. 8d). The spectrum is a plot of the strength of singularities present in the data ( $\alpha$ ) on the  $x$ -axis v. their local fractal dimension ( $D$ ) as  $f(\alpha)$  on the  $y$ -axis. The greater the number of distinct

## QUANTIFYING HYDROTHERMAL SYSTEMS

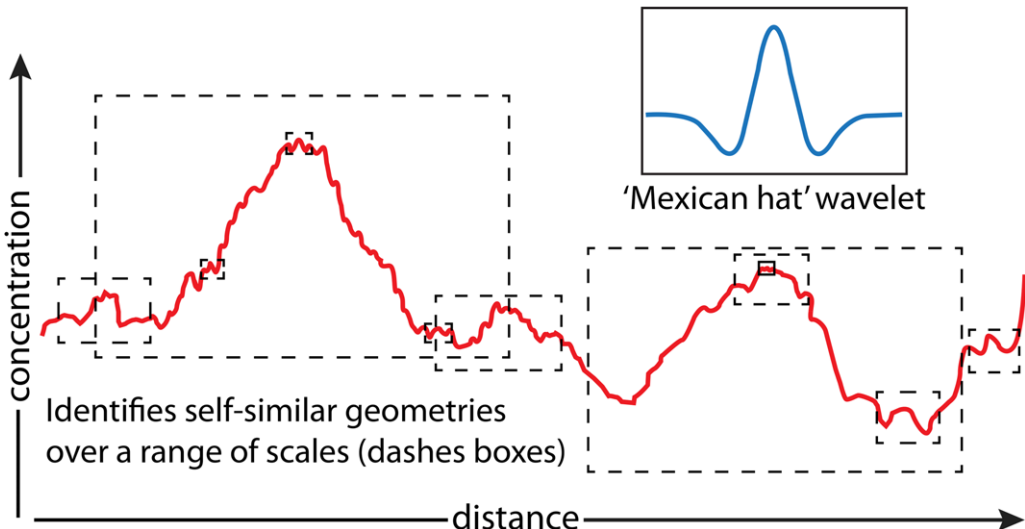


**Fig. 7.** Visual representation of how a wavelet is applied to a signal, here the Mexican hat wavelet (second derivative of the Gaussian distribution). The wavelet size (wavelength) is progressively increased, with each size scanned incrementally across the signal. During each scan, the wavelet determines the degree to which each successive increment of the dataset matches its form, returning a coefficient. These coefficients are used to construct a wavelet transform scalogram, such as that shown in Fig. 8b.

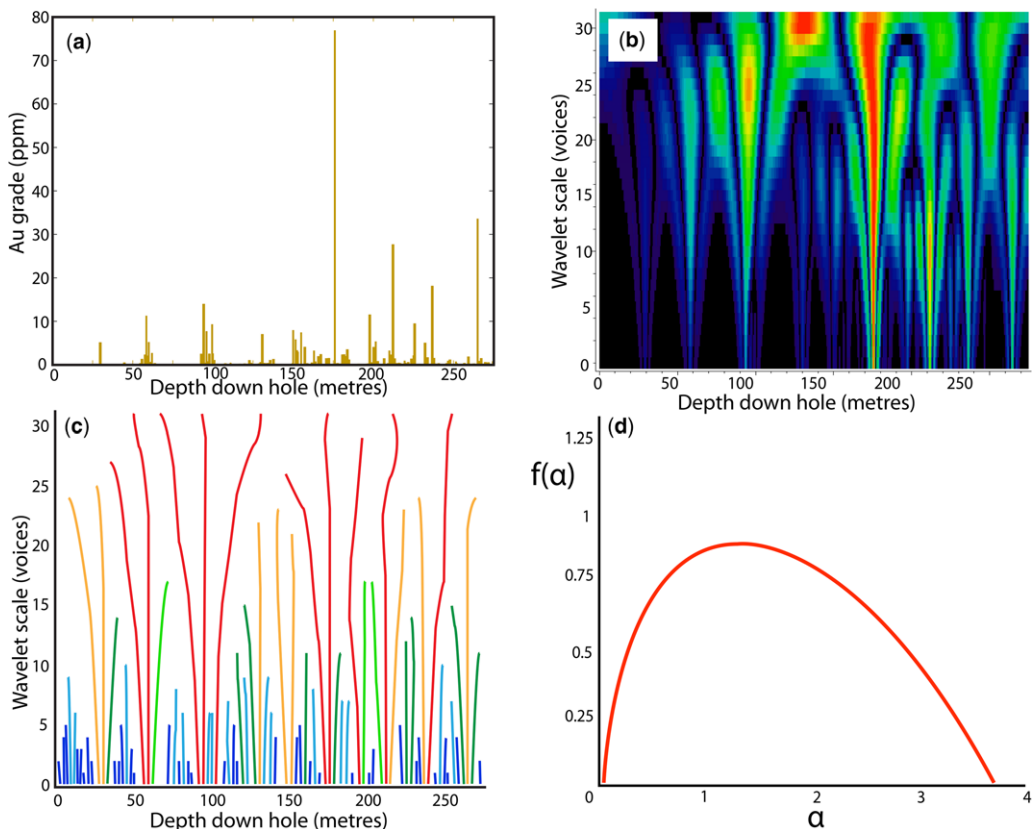
groups of singularities present in the signal, the greater the  $\alpha$  range of the singularity spectrum along the  $x$ -axis. The spectrum is so-called because each of the fractal dimensions it encompasses is a singular function (i.e. a mathematical function that is discontinuous, or cannot be differentiated).

Figure 8 demonstrates the key stages of the WTMM method of determining the singularity spectrum (Fig. 8d), as applied to an example Au assay signal from Sunrise Dam using the Mexican hat wavelet. During each scan the wavelet assesses the degree to which each successive increment of the dataset matches its form, returning coefficients that are used to construct a wavelet transform scalogram (Fig. 8b). The wavelet scalogram provides a visual reference of how the signal correlations behave with varying scale. These behaviours are distilled into an extrema, or skeleton, plot (e.g. Fig. 8c) that illustrates how the local maxima or extrema in the scalogram vary with scale. All extrema lines extend upwards from the lowest wavelet scale (one voice) and are detectable on variable wavelet scales. At smaller scales of analysis a greater number of high-frequency, low-wavelength correlations are made. As the scale of analysis increases, the local maxima (correlations) progressively decrease in number, but increase in wavelength.

The singularity spectrum is calculated by first computing the partition function  $Z(q, a)$  of the skeleton plot in Figure 8c. Linear regressions are then applied to the partition function to determine the

power law scaling exponents, or  $\tau(q)$ , for the scaling behaviours present. The local fractal dimension,  $f(\alpha)$ , for each set of singularities is then calculated by the Legendre transform of  $\tau(q)$  and plotted against  $\alpha$  (singularity strength) on the singularity spectrum. In this study, these procedures were carried out using LastWave 3.1 software (Arneodo *et al.* 2003; Bacry 2009). A detailed definition and discussion of the WTMM method and the calculations performed by the software are available in Hobbs & Ord (2015) and Ord *et al.* (2016).

*Interpreting the singularity spectrum of a multifractal.* Figure 9a presents the key features of the singularity spectrum that may be used to quantify the system. The range of the singularity spectrum is a function of the number of individual fractal dimensions ( $D$  values, or scaling law exponents) that describe the dynamics of the system. Systems in which all sub-signals correlate over similar length scales and amplitudes (i.e. the signal is relatively regular) will be characterized by a narrow range of singularity spectrum. Conversely, a system in which the sub-signals correlate over a diverse range of scales will be characterized by a broad singularity spectrum (i.e. a greater number of fractal dimensions). The range of the singularity spectrum is therefore an important quantity for comparing the dynamics of signals. In the context of downhole abundance data, a narrow singularity spectrum represents relatively regular fluctuations in mineral



**Fig. 8.** Wavelet-based analysis of a signal to quantify its multifractal spatial dynamics. (a) Example downhole Au assay signal from the Sunrise Dam hydrothermal system. (b) Wavelet transform scalogram derived from application of the Mexican hat wavelet to signal part (a). The wavelet scale increases up the *y*-axis and is expressed in voices as defined in this paper. Black to dark blue indicates a poor match between the wavelet and signal; yellow to red indicates the strongest match. (c) An extrema, or skeleton, plot derived from a wavelet transform scalogram, here the example in part (b). The extrema plot maps out the spatial organization of local maxima (best fits) on the wavelet scalogram. The extrema lines are colour-coded according to the wavelet scale that they extend upwards to on the *y*-axis. Dark blue = 0–5 voices; light blue = 5–10 voices; dark green = 10–15 voices; light green = 15–20 voices; orange = 20–25 voices; red  $\geq$  25 octaves. The extrema plot extracted from a wavelet transform scalogram is used to calculate a singularity spectrum. (d) Singularity spectrum derived from the extrema plot in part (c).  $\alpha$  increases along the *x*-axis and is a measure of the strength of singularities present.  $f(\alpha)$  on the *y*-axis is the local fractal dimension ( $D$ ) of each group of singularities. Important metrics of the spectrum used to quantify the system are presented in Figure 9.

phase or element concentration that occur over similar wavelengths and amplitudes. A broad singularity spectrum represents more intermittent and irregular fluctuations in concentration that occur over a greater range of length scales and amplitudes.

The range of a singularity spectrum is subdivided into two key components: a left limb and a right limb (Fig. 9a). The left and right limbs of a singularity spectrum describe different aspects of the system – the dynamics of the highest and lowest probability values present, respectively. Where the high and low probability components of a signal have a similar scaling complexity to one another,

the singularity spectrum will be approximately symmetrical (i.e. both limbs are of a similar span). Where either of these components shows more complexity than the other, the singularity spectrum becomes asymmetrical, with one limb broader than the other. Therefore the left limb width, right limb width and spectrum asymmetry are important characteristics for quantifying the spatial organization of elements or phases in hydrothermal systems. We present here a method for quantifying the degree of symmetry of a singularity spectrum (Fig. 9b), allowing an objective comparison between spectra. Spectrum asymmetry is defined here as the percentage

## QUANTIFYING HYDROTHERMAL SYSTEMS

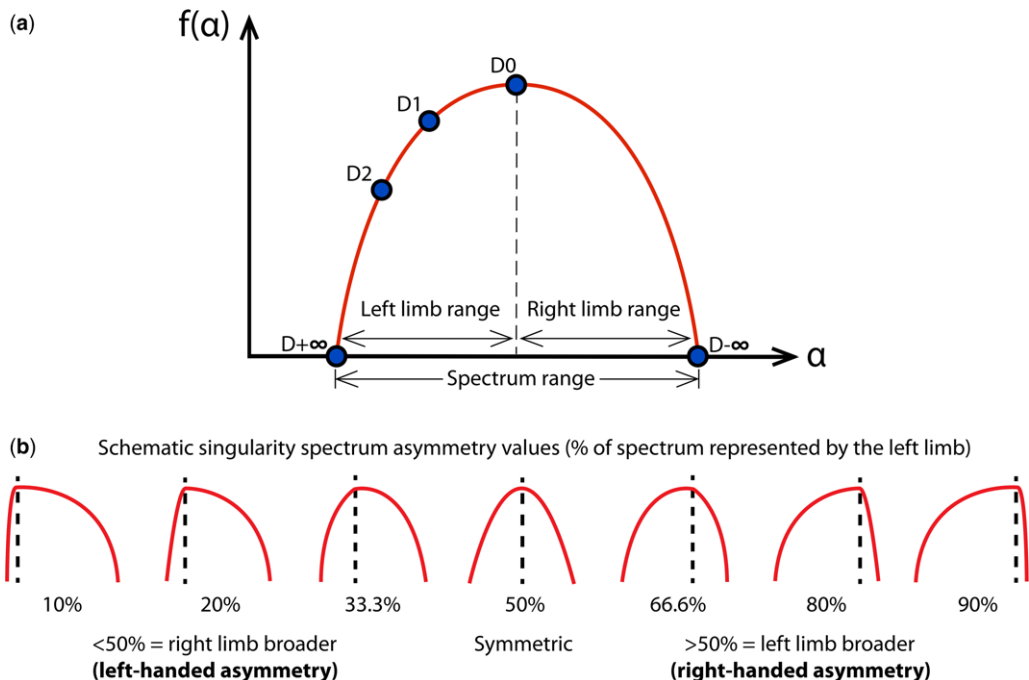


**Fig. 9.** (a) Commonly used singularity spectrum metrics. The spectrum range quantifies the range of fractal dimensions ( $D$ , or scaling law exponents) describing the spatial dynamics of the signal. The broader the singularity spectrum, the greater the number of scaling law exponents required to describe the signal. The left limb range quantifies the spatial dynamics of the most common (high probability) values in the signal; the right limb range quantifies the spatial dynamics of the least common (lower probability) values. (b) A newly defined method for quantifying the degree of asymmetry of a singularity spectrum, allowing a straightforward comparison between different spectra. The asymmetry values are defined as the percentage that the left limb constitutes of the entire spectrum range. The values may equally be considered as the normalized  $\alpha$ -position of  $D_0$  (the apex of the spectrum) across the span of the spectrum.

that the left limb ( $D_{+\infty}$  to  $D_0$ ) constitutes of the entire spectrum range. This normalized percentage is an informative measure because it also represents the  $\alpha$  position of  $D_0$  (the most frequent value of singularity strength) across the span of the spectrum. Using this system, a perfectly symmetrical spectrum has an asymmetry measure of 50%. Where the left-hand limb is broader, the measure is  $>50\%$ ; this is referred to as right-handed asymmetry. Where the right-hand limb is broader, the measure is  $<50\%$ ; this is referred to as left-handed asymmetry. The greater the asymmetry measure deviates from 50%, the greater the spectrum asymmetry. A schematic illustration of standard spectrum asymmetry values is included alongside the spectrum asymmetry data for each ore body throughout.

Other key singularity spectrum attributes used to quantify the system are  $D_0$ ,  $D_1$ ,  $D_2$ ,  $D_{+\infty}$  and  $D_{-\infty}$  (Fig. 9a).  $D_{+\infty}$  and  $D_{-\infty}$  are the left- and right-hand extremities of the spectrum where it connects with the  $\alpha$ -axis.  $D_0$  (referred to as the capacity dimension) is the point at the apex of the spectrum, with

a tangent of 0, where the left and right limbs meet.  $D_1$  and  $D_2$  are points on the spectrum with tangents of 1 and 2, respectively (Arneodo *et al.* 1995).  $D_1$  (the information dimension) relates to Shannon's entropy and may be used as a measure of the uniformity of data density (i.e. how it changes with scale) (Salat *et al.* 2017). The greater the value of  $D_1$ , the more uniform the data density.  $D_2$  (the correlation dimension) can be used to provide a measure of how scattered the data is and determines the probability that pairs of independent events occur in the same 'box'. The greater the value of  $D_2$ , the greater the degree of compactness of the data. For the purposes of this study,  $D_1$  and  $D_2$  are simply used as reference markers on the left limb of the singularity spectrum to further compare spectra. Their thermodynamic significance will be explored in detail in future contributions.

*Wavelet analysis of Sunrise Dam drillcore.* Wavelet analysis of the Sunrise Dam drillcores was carried out using the free software LastWave 3.1 for

Windows (Arneodo *et al.* 2003; Bacry 2009). The well-established Mexican hat wavelet (the second derivative of the Gaussian distribution) was selected because its shape is applicable to the peaks and troughs in concentrations commonly observed in the Au assay and hyperspectral mineral abundance datasets. The scale-adapted method of WTMM was used (Arneodo *et al.* 1995), which uses varying sizes of the mother wavelet. Consistent wavelet parameters were applied to all drillcores within an individual ore body. A three-octave, eight-voice, setup was applied to drillcores in GQ and Cosmo East. This three-octave setup was selected because it is the maximum applicable wavelet size range allowed by the LastWave software for the length of most drillcores in these ore bodies. An analysis resolution of eight voices was selected because it allows good resolution of the resulting wavelet transform scalograms. Most of the drillcores intersecting the Vogue ore body are greater in length than those in GQ and Cosmo East and therefore a greater wavelet size range of four octaves, at a resolution of eight voices, was applied to optimize the analysis. The absolute values of the singularity spectrum metrics for Vogue cannot therefore be straightforwardly compared with those from GQ and Cosmo East. However, the behaviour of individual phases in Vogue relative to one another can be compared with the relative behaviour of the respective mineral phases in the other two ore bodies.

### Hurst exponent analysis: assessing long-range correlations

Wavelet transform scalograms (e.g. Fig. 8b) provide a visual assessment of signal behaviour across varying scales of examination. As demonstrated in the preceding section, singularity spectrum analysis of a wavelet transform can be used to quantify correlations between different signal components and the range of scaling law exponents that apply to them. However, a wealth of other information may also be extracted from the scalogram. Hurst exponents (Feder 1988; Arneodo *et al.* 2002, 2003; Sprott 2003) are one such example. Hurst exponents may be used to quantify the degrees of local-scale irregularity (or roughness) in the signal and how these scale with varying distance across the drillcore. In other words, they assess how different signal components correlate at different length scales. Importantly, this evaluates the length scales at which long-range correlations are present in the system. Hurst exponents, coupled with singularity spectra determination, have been applied to different mineralization styles (Liu *et al.* 2012; Sun & Liu 2014; Ord *et al.* 2016).

In this study, alteration minerals and Au were examined as one-dimensional series of concentrations,  $\xi$ , which vary with distance ( $d$ ) down the drillcore. Calculating the Hurst exponent (see visual summary in Fig. 10a) first involves determining the mean of  $\xi$ , followed by the cumulative departures from this mean to obtain  $\Xi(d)$ . Then, if  $R(d)$  is the difference between the largest and smallest values of  $\Xi$ , and  $\sigma(d)$  is the standard deviation of  $\xi$ , then the Hurst exponent ( $H$ ) for the dataset is:

$$\frac{R(d)}{\sigma(d)} = \left(\frac{d}{2}\right)^H$$

This definition of the Hurst exponent considered its application to the raw concentration data for a phase or element. This provides a quantification of behaviour at a set scale. However, this study is concerned with quantifying how mineral or element behaviour within a drillcore changes with varying scales. This is achieved by taking different transect profiles across a wavelet transform scalogram at progressively increasing wavelet scales (e.g. Fig. 10b, c) and calculating a Hurst exponent for the data extracted at each scale. The value of the Hurst exponent for each transect lies in the range  $0 < H < 1$ , the significance of which is summarized in Table 2 (Ord *et al.* 2016).

Hurst exponents tend to increase in value with increasing wavelet scale, commonly transitioning from  $0 < H < 0.5$  (long-range positive correlations are absent) to  $0.5 < H < 1$ . Low values are associated with high degrees of signal roughness; high values with progressively smoother signals. The threshold  $H = 0.5$  is important in defining the onset of long-range positive correlations (Sprott 2003). Plots are made of wavelet scale (or absolute scale, if known) v.  $H$ . The scale at which long-range positive correlations are present is marked by two criteria: (1) a significant rate of increase in the value of  $H$ ; and (2)  $H \geq 0.5$ . For many signals, the significant rate of increase in  $H$  occurs at, or below, the intersection of the  $H = 0.5$  threshold. Other datasets may have flat trajectories of  $H \approx 0.5$  ( $\pm c. 0.05$ ) in advance of the significant rate of increase. Hurst exponent determination is fast and convenient.

Four key Sunrise Dam drillcores were selected for Hurst exponent analysis following completion of the wavelet-based analysis. For each hole, Hurst exponents were determined for Au, sericite, chlorite, calcite and ankerite at each wavelet scale to assess the scales of onset of long-range correlation in each. The wavelet scalograms and Hurst exponents used to assess long-range correlations were calculated using Mathematica (<https://www.wolfram.com/mathematica/>).

## QUANTIFYING HYDROTHERMAL SYSTEMS

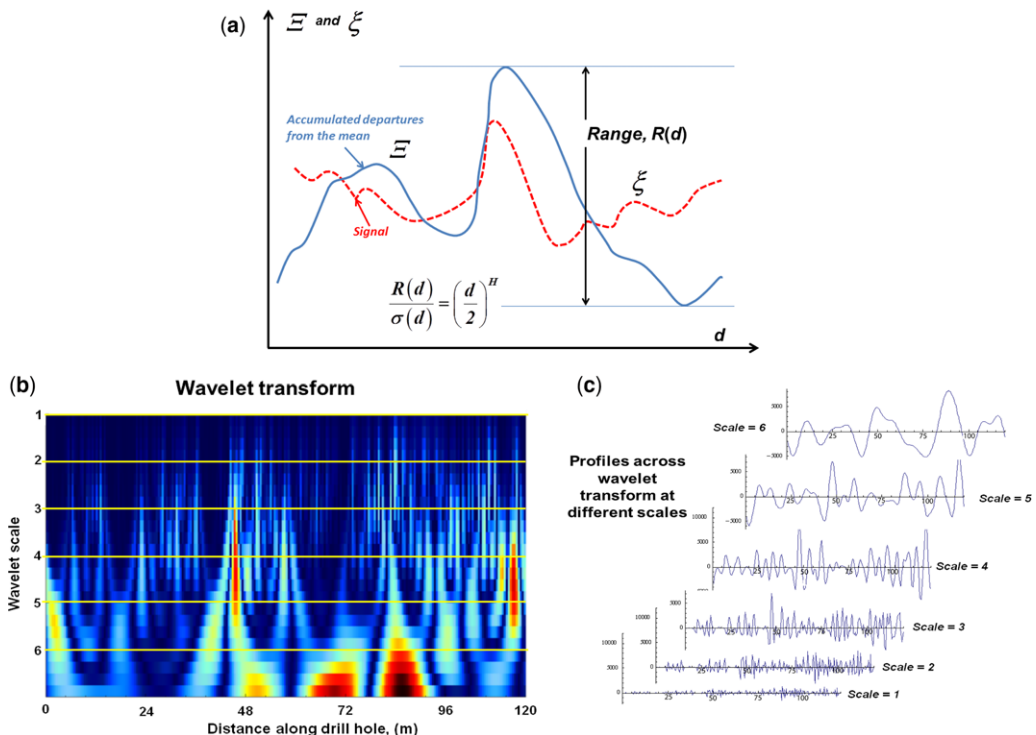


**Fig. 10.** (a) Definition of the Hurst exponent,  $H$ .  $\xi$  on the y-axis (dashed line) is the initial data signal as a function of distance ( $d$ ) along the x-axis.  $\Xi$  (also y-axis) is derived from these data as the cumulative departure of the data from the mean.  $\sigma$  is the standard deviation of  $\xi$ . After Feder (1988). (b) Wavelet transform scalogram derived from a 0.5 m resolution downhole chlorite hyperspectral abundance dataset. Wavelet scale along the y-axis is in octaves (increasing from top to bottom), with scales 1–6 marking the start of each octave. Each octave is subdivided into four voices, each represented by an individual block or pixel. (c) Series of section profile transects across the wavelet scalogram over a range of wavelet scales, corresponding to the section lines across the scalogram in part (b). Note that the wavelengths of correlation in the signal increase with scale and the profiles become progressively smoother. Modified from Ord *et al.* (2016).

## Results

### Wavelet analysis of hyperspectral data in individual ore bodies

We report here the singularity spectra for Au from 181 drillcores, chlorite from 193 drillcores, sericite

from 183 drillcores, calcite from 193 drillcores, ankerite from 197 drillcores and amphibole from 130 drillcores. The following sections present key singularity spectrum metrics ( $D_{+\infty}$ ,  $D_{-\infty}$ ,  $D_0(\alpha)$ ,  $D_1(\alpha)$ ,  $D_2(\alpha)$ , spectrum range, left limb range, right limb range and spectrum asymmetry) for Au and each phase within an ore body. Visual

**Table 2.** Characteristics of the Hurst exponent ( $H$ ) for a one-dimensional signal (after Ord *et al.* 2016)

$H$	Meaning	Pattern characteristics
$0.5 < H < 1$	Persistent	Long-range positive autocorrelations A high (low) value tends to be followed by another high (low) value. The overall trend is to higher (lower) values. Power law decay in autocorrelations.
$H = 0.5$	Completely uncorrelated sequence	Autocorrelations at small intervals can be positive or negative. Absolute value of autocorrelations decays rapidly to zero.
$0 < H < 0.5$	Antipersistent	Long-range switching between high and low values A high value tends to be followed by a low value. Power law decay in autocorrelations.

definitions of each metric are provided in Figure 9. Spectrum range is a measure of the strength of multifractality (i.e. the number of distinct groups of singularities present, each with its own fractal dimension). Left limb range quantifies the number of fractal dimensions that describe the dynamics of the highest probability values present; right limb range quantifies the number of fractal dimensions that describe the dynamics of the lowest probability values present. A schematic illustration of different spectrum asymmetry values is included with the asymmetry histograms of each ore body for reference. Each individual metric is presented as a series of frequency-normalized histograms of its distribution in each phase within an ore body. In the following sections, the relative behaviour of all phases within each individual ore body is compared, then the behaviour relative to their respective counterparts in other ore bodies.

#### *Singularity spectra for GQ ore body lodes*

Individual mineral phases and Au in GQ show distinct behaviour in many singularity spectrum metrics. Each phase displays considerable variation in singularity spectrum range between drillcores throughout the ore body (Fig. 11). Chlorite spectrum ranges peak at c. 1.75 and display the greatest variability, with individual spectra ranging from 0.5 to c. 4.5. Calcite and ankerite display highly similar spectrum range behaviour, both having end-members extending from 1 to 3.25 and peaking in the range 1.5–2.25. Au displays the highest modal spectrum range of all the minerals in GQ (c. 2.75). Sericite has the lowest modal spectrum range of all phases (0.75–1.25) and also the most restricted range profile (dominantly 0.5–2, with a few >2). Amphibole has a modal peak at c. 1.5, similar to that in chlorite.

Au has the greatest left limb ranges of all spectra measured (Fig. 11) peaking between 0.75 and 1.75. Sericite and chlorite have the narrowest left limb ranges, peaking at 0.25–0.5 and 0.25–0.75, respectively. Amphibole, ankerite and calcite have left limb ranges intermediate to those of Au (broad) and sericite and chlorite (narrow). Sericite and amphibole have the narrowest right limb ranges (Fig. 11), both peaking between 0.5 and 0.75. Au also has the greatest modal peak in right limb range (1.25–1.5). Chlorite shows the most broadly distributed variation in right limb range of all phases (0.5–2).

Mineral phases in GQ also display distinct singularity spectrum asymmetries (Fig. 12). Au and amphibole have approximately equal proportions of left- and right-handed spectra, with end-member asymmetry values of 20% and c. 80%. Both display modal peaks across the 50% symmetry marker (i.e. the majority are close to symmetrical). Calcite and

ankerite display highly similar distributions, characterized by almost exclusively (weak to moderate) left-handed asymmetries in the range 20–50%. Chlorite and sericite also display almost exclusively left-handed asymmetry. However, they display much broader profiles with substantial proportions of spectra characterized by extreme asymmetry values between 10 and 25%.

$D_0(\alpha)$ ,  $D_1(\alpha)$ ,  $D_2(\alpha)$ ,  $D_{+\infty}$  and  $D_{-\infty}$  positions for all spectra measured from GQ are provided in Table 3.

In summary, calcite and ankerite in GQ display similar singularity spectrum signatures. Both have similar modal peaks and distributions in spectrum range, weak to moderate left-handed asymmetry, intermediate left and right limb ranges, and intermediate  $D_1(\alpha)$  and  $D_2(\alpha)$  values. Au displays the greatest singularity spectrum range (i.e. the strongest multifractal signature), the lowest values of  $D_1(\alpha)$ ,  $D_2(\alpha)$  and  $D_{+\infty}$ , and both left- and right-handed asymmetry. Sericite and chlorite within GQ display similar behaviour in many spectrum metrics, having the highest  $D_1(\alpha)$ ,  $D_2(\alpha)$  and  $D_{+\infty}$  values, and the greatest spectrum asymmetry (almost exclusively left-handed). Sericite shows the lowest spectrum ranges of any phase, whereas chlorite shows the broadest spectrum range distribution. All phases, with the exception of Au, show similar distributions in  $D_0(\alpha)$ .

#### *Singularity spectra for Vogue ore body lodes*

Mineral phases in Vogue also display distinguishing singularity spectrum characteristics. Sericite and chlorite display the broadest distributions in spectrum range (Fig. 13). Chlorite is multi-modal, with four modes of approximately equal strength at 1.5, 2.25, 3 and 3.75 (the last being marginally stronger). Sericite is bimodal with a narrow peak at 0.75 and a broader one spanning c. 2–3. Au displays a narrow distribution in spectrum range (the majority extending between c. 2 and 3) and peaks at 2.25. Amphibole has the lowest modal peak of all phases (1.5), with a narrow distribution ranging from c. 1 to 2.5. Calcite and ankerite show similar spans in distribution and peak between 1.5 and 2.25.

Au has the broadest left limb range (peaking between 1 and 1.5); sericite has the narrowest (peaking between 0.25 and 0.75) (Fig. 13). Calcite, ankerite, chlorite and amphibole have predominantly intermediate values between the peaks of Au and sericite. Chlorite and sericite have the broadest, and most diverse, right limb ranges (Fig. 13). Sericite right-hand limbs ranging from 0 to 2.75; chlorite ranges from 0.5 to 3.5. Amphibole has the narrowest right limb ranges, peaking between 0.5 and 0.75. Ankerite and calcite have similar right limb width peaks between 1 and 1.5.

## QUANTIFYING HYDROTHERMAL SYSTEMS

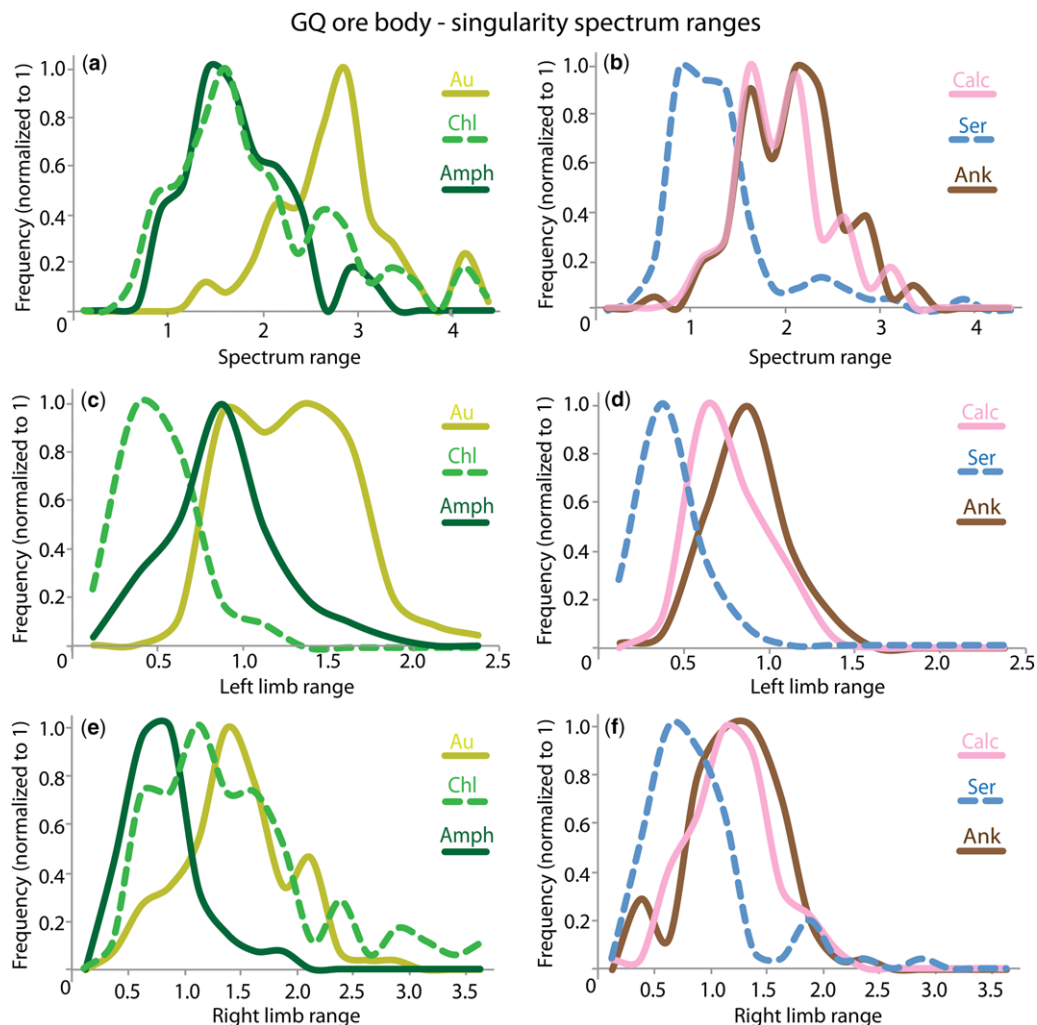


**Fig. 11.** Frequency-normalized histograms of (a, b) singularity spectrum range, (c, d) left limb range and (e, f) right limb range for Au and all mineral phases in GQ. Au has the highest mode in the spectrum range; sericite has the lowest. Chlorite and amphibole also show low modes in the spectrum range, slightly higher than sericite. Calcite and ankerite show intermediate spectrum range modes. Au has the broadest left-hand limbs; chlorite and sericite have the narrowest. Calcite, ankerite and amphibole have intermediate left-hand limb widths. Sericite and amphibole have the narrowest right limb ranges; Au and chlorite show the greatest variability in right-hand limb width. Calcite and ankerite have intermediate right-hand limb widths, with less variation than Au and chlorite. Bin width for all plots = 0.25. Number of samples: Au, 102; chlorite, 97; amphibole, 82; sericite, 88; ankerite, 101; and calcite, 98.

Au singularity spectra in Vogue show relatively weak asymmetry (mostly between 30 and 70%), with almost equal proportions of left- and right-handed (Fig. 14). Calcite and ankerite show a strong predominance of left-handed asymmetry (weak to moderate), dominantly extending from values of 20 to 50%. Sericite and chlorite display the most extreme asymmetries of all phases and are almost exclusively left-handed. Both display a substantial proportion of spectra with strong asymmetries

<25%. Rare end-members in chlorite extend to extreme values <10%. Strong left-handed asymmetries in sericite and calcite are consistent with them having the broadest right limb ranges.

$D_0(\alpha), D_1(\alpha), D_2(\alpha), D_{+\infty}$  and  $D_{-\infty}$  positions for all spectra measured from Vogue are provided in Table 4.

In summary, chlorite and sericite in Vogue show relatively similar singularity spectrum characteristics. Both phases display the greatest variations in

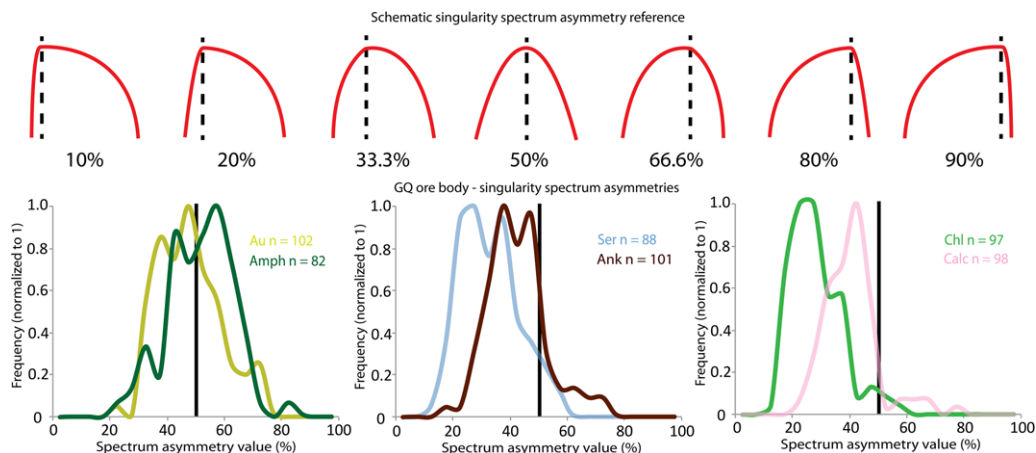


**Fig. 12.** Frequency-normalized histograms of spectrum asymmetry values in Au and all mineral phases in GQ. Reference figure in upper panel shows schematic examples of different asymmetry values. Asymmetry values are the percentage of the entire spectrum composed by the left limb and may also be considered the normalized  $\alpha$  position of  $D_0$  (the most common singularity strength) across the range of the spectrum. Values  $<50\%$  express that the right limb is broader; values  $>50\%$  that the left is broader. Au and amphibole have roughly equal proportions of left- and right-handed asymmetry. Calcite and ankerite have almost exclusively left-handed asymmetry (weak to moderate). Chlorite and sericite are almost exclusively left-handed, with the greatest proportions of extreme asymmetries. Bin width = 5%.  $n$  = number of individual drillhole results.

singularity spectrum range. Many of their occurrences are the most strongly hierarchical structures in the ore body, with spectrum ranges  $\geq 2.5$ . They also display the strongest asymmetry of all phases (both almost exclusively left-handed) and have the highest  $D_{+\infty}$ ,  $D_1(\alpha)$  and  $D_2(\alpha)$  values. Au has the lowest  $D_{+\infty}$ ,  $D_1(\alpha)$  and  $D_2(\alpha)$  values, relatively low variations in spectrum range (peaking between 2 and 3) and relatively weak asymmetry (both

left- and right-handed). Calcite and ankerite in Vogue display spectrum range modal peaks (c. 1.5–2.25), spectrum range end-members (c. 1–3) and spectrum asymmetry (a dominance of weak to moderately left-handed). Calcite has higher modes in  $D_{+\infty}$ ,  $D_1(\alpha)$  and  $D_2(\alpha)$  values than ankerite. Amphibole has intermediate  $D_{+\infty}$ ,  $D_1(\alpha)$  and  $D_2(\alpha)$  values, the lowest mode in spectrum range and both weak left- and right-handed asymmetry.

**Table 3.** Singularity spectrum metrics for Au and key mineral phases in GQ (all drillcores)

	No. of samples	$D_0(\alpha)$	$D_1(\alpha)$	$D_2(\alpha)$	$D_{+\infty}$	$D_{-\infty}$
Au	103	0.9–2.5 (1.25–1.5)	0.01–1.16 (0.25–0.5)	0–1.04 (0–0.25)	0–0.93 (0–0.25)	1.47–4.47 (2.5–2.75)
Sericite	89	0.82–1.65 (1–1.25)	0.69–1.39 (0.75–1.25)	0.61–1.28 (0.75–1)	0.48–1.15 (0.75–1)	1.24–4.53 (1.75–2)
Chlorite	97	0.89–1.9 (1–1.5)	0.46–1.33 (0.75–1.25)	0.45–1.28 (0.75–1)	0.35–1.21 (0.75–1)	1.35–5.18 (2–2.25)
Calcite	98	0.77–1.59 (1–1.25)	0.42–1.19 (0.5–0.75)	0.04–1.07 (0.25–0.75)	0.03–0.85 (0.25–0.5)	1.24–3.5 (1.75–2.5)
Ankerite	101	0.78–1.59 (0.75–1.25)	0.37–1.01 (0.5–0.75)	0.01–0.83 (0.25–0.5)	0–0.69 (0–0.25)	1.23–3.5 (1.75–2; 2.25–2.75)
Amphibole	82	0.75–2.25 (1–1.5)	0.12–1.25 (0.5–0.75)	0–1.4 (0.25–0.5)	0.01–1 (0–0.25)	1.23–3.85 (1.75–2.25)

Frequency distribution end-members for each spectrum metric are given first; numbers in parentheses are the modal peak on the frequency histogram.

## QUANTIFYING HYDROTHERMAL SYSTEMS

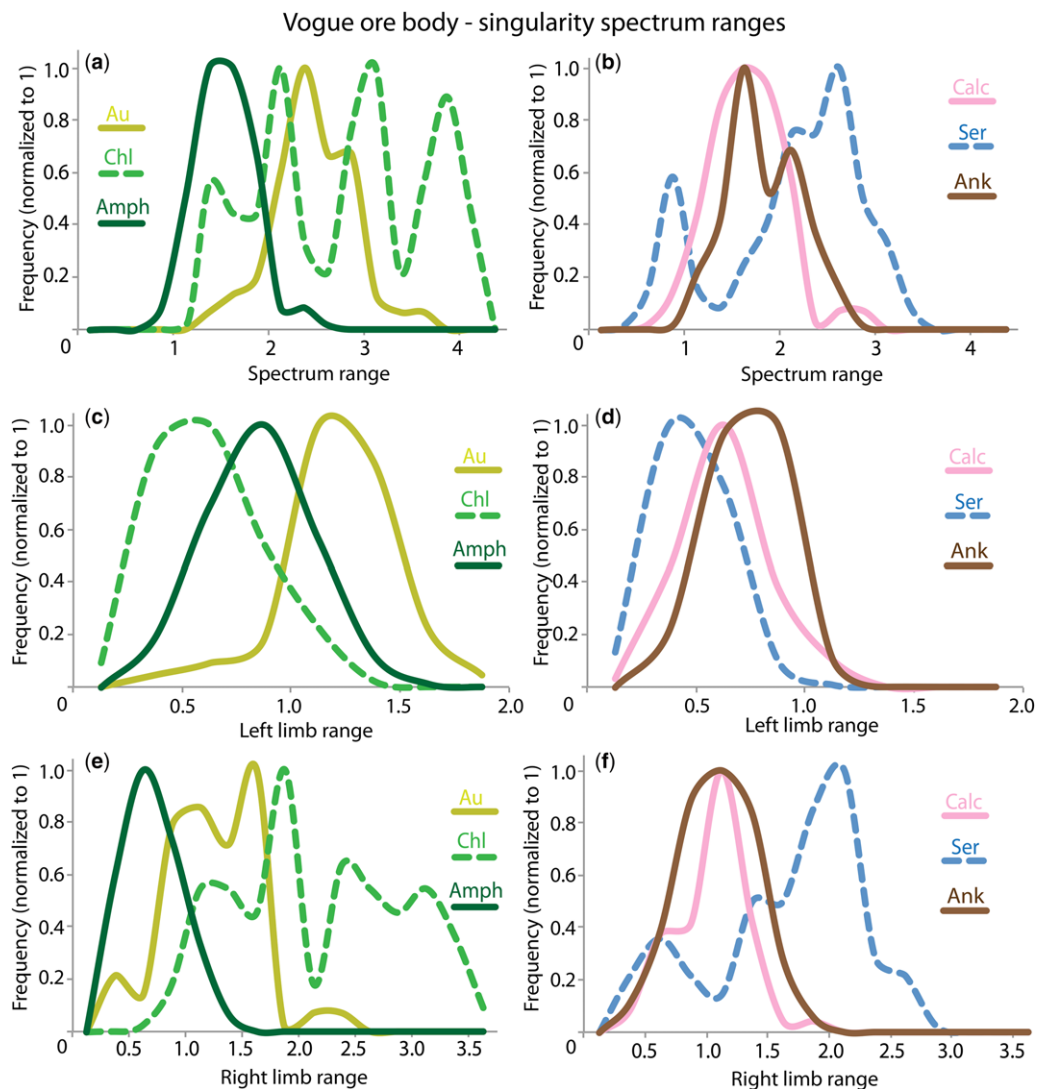


**Fig. 13.** Frequency-normalized histograms of (a, b) singularity spectrum range, (c, d) left limb range and (e, f) right limb range for Au and all mineral phases in Vogue. Chlorite and sericite have the broadest variation in the spectrum range. Chlorite is multi-modal and has some of the broadest ranges of all spectra measured. Broad spectra ranges in sericite are similar to those in Au. Amphibole has the lowest modal peak in the spectrum range. Calcite and ankerite have intermediate spectrum ranges. Au has the broadest left-hand limbs, sericite the narrowest. Calcite, ankerite, amphibole and chlorite have intermediate left limb widths. Chlorite and sericite have the broadest and most diverse right limb widths. Amphibole has the narrowest right-hand limbs. Au, calcite and ankerite have similar intermediate right limb ranges. Bin width for all plots = 0.25. Number of samples: Au, 54; chlorite, 62; amphibole, 41; sericite, 61; ankerite, 64; and calcite, 57.

#### Singularity spectra for Cosmo East ore body lodes

Chlorite in Cosmo East has the narrowest singularity spectrum ranges of all phases (Fig. 15), with a strong peak in the range 1–1.25. Fewer occurrences have ranges between 1.5 and 3. Sericite also shows a

strong peak in the range 1–1.25; however, it is more strongly multi-modal than chlorite, with a greater proportion of spectrum ranges >1.5. The Au singularity spectrum ranges peak between 2.5 and 2.75, with end-members extending from c. 1 to 4. Ankerite has a relatively narrow spectrum range profile between c. 1.5 and 3, with two sub-peaks at

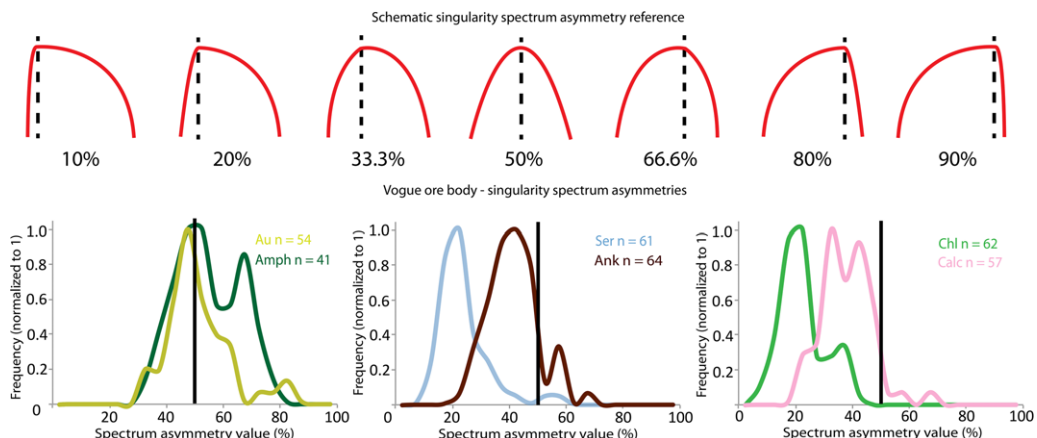


**Fig. 14.** Frequency-normalized histograms of spectrum asymmetry values in Au and all mineral phases in Vogue. Reference figure in upper panel shows schematic examples of different asymmetry values. Au has roughly equal proportions of left- and right-handed asymmetry. Amphibole also has large proportions of left- and right-handed asymmetry. Calcite and ankerite have a predominance of weak to moderate left-handed asymmetry. Sericite and chlorite have weak to strong left-handed asymmetry (almost exclusive). Bin width = 5%.  $n$  = number of individual drillhole results.

1.75–2 and 2.5–2.75. Calcite shows a broad peak between 1 and 2.75 (strongest in the range 2–2.5) and a narrower peak between 3 and 3.25.

Chlorite and sericite display the narrowest left limb ranges of all phases (Fig. 15), peaking in the range 0.25–0.5. Au has the broadest left limb ranges, peaking between 1 and 1.5. Calcite and ankerite have intermediate left limb ranges, peaking at 0.5–0.75 and 0.75–1.25, respectively. Right limb widths in chlorite and sericite are generally the narrowest of all phases (Fig. 15), peaking at 0.5–0.75 and 0.75–1, respectively. Sericite has an additional (lower strength) peak between 1.5

and 2. Right-hand limbs in Au range between 0 and 1.75, peaking between 1 and 1.25. Ankerite right-hand limbs range between 0.5 and 1.75, with two peaks at 0.75–1 and 1.25–1.5. Calcite right-hand limbs range from 0.5 to 2.25, with the strongest peak between 1 and 1.5 and a second peak between 2 and 2.25.

Au singularity spectra display multi-modal asymmetry (Fig. 16), extending from strongly right-handed (85%) to moderately left-handed (25%). The majority are weakly to strongly right-handed. Chlorite displays exclusively left-handed asymmetry from weak (45%) to strong (10%). The greatest

**Table 4.** Singularity spectrum metrics for Au and key mineral phases in Vogue (all drillcores)

	No. of samples	$D_0(\alpha)$	$D_1(\alpha)$	$D_2(\alpha)$	$D_{+\infty}$	$D_{-\infty}$
Au	59	0.88–1.99 (1.25–1.5)	0.04–0.9 (0.25–0.5)	0–0.78 (0–0.25)	0–0.72 (0–0.25)	1.82–3.63 (2.25–3)
Sericite	69	0.87–1.78 (1–1.25)	0.72–1.18 (0.75–1)	0.63–1.1 (0.75–1)	0.42–0.99 (0.75–1)	1.23–4.19 (2.75–3.75)
Chlorite	72	0.93–1.77 (1.25–1.5)	0.62–1.16 (0.75–1)	0.46–1.13 (0.75–1)	0.28–0.99 (0.5–0.75)	2.01–4.96 (2.25–2.5; 3–3.25; 3.5–3.75; 4.5–4.75)
Calcite	70	0.8–1.38 (1–1.25)	0.52–0.91 (0.5–1)	0.16–0.86 (0.5–0.75)	0.07–0.73 (0.25–0.5)	1.23–3.08 (2–2.25)
Ankerite	78	0.69–1.38 (1–1.25)	0.43–0.96 (0.5–0.75)	0.08–0.84 (0.25–0.5)	0–0.7 (0–0.25)	1.44–3.08 (2–2.5)
Amphibole	48	1.03–1.66 (1.25–1.5)	0.44–1.28 (0.5–1)	0.04–1.19 (0.25–0.5)	0.04–1.04 (0.25–0.5)	1.61–2.53 (1.75–2.25)

Frequency distribution end-members for each spectrum metric are provided first; numbers in parentheses are the modal peak on the frequency histogram.

## QUANTIFYING HYDROTHERMAL SYSTEMS

## Cosmo East ore body - singularity spectrum ranges

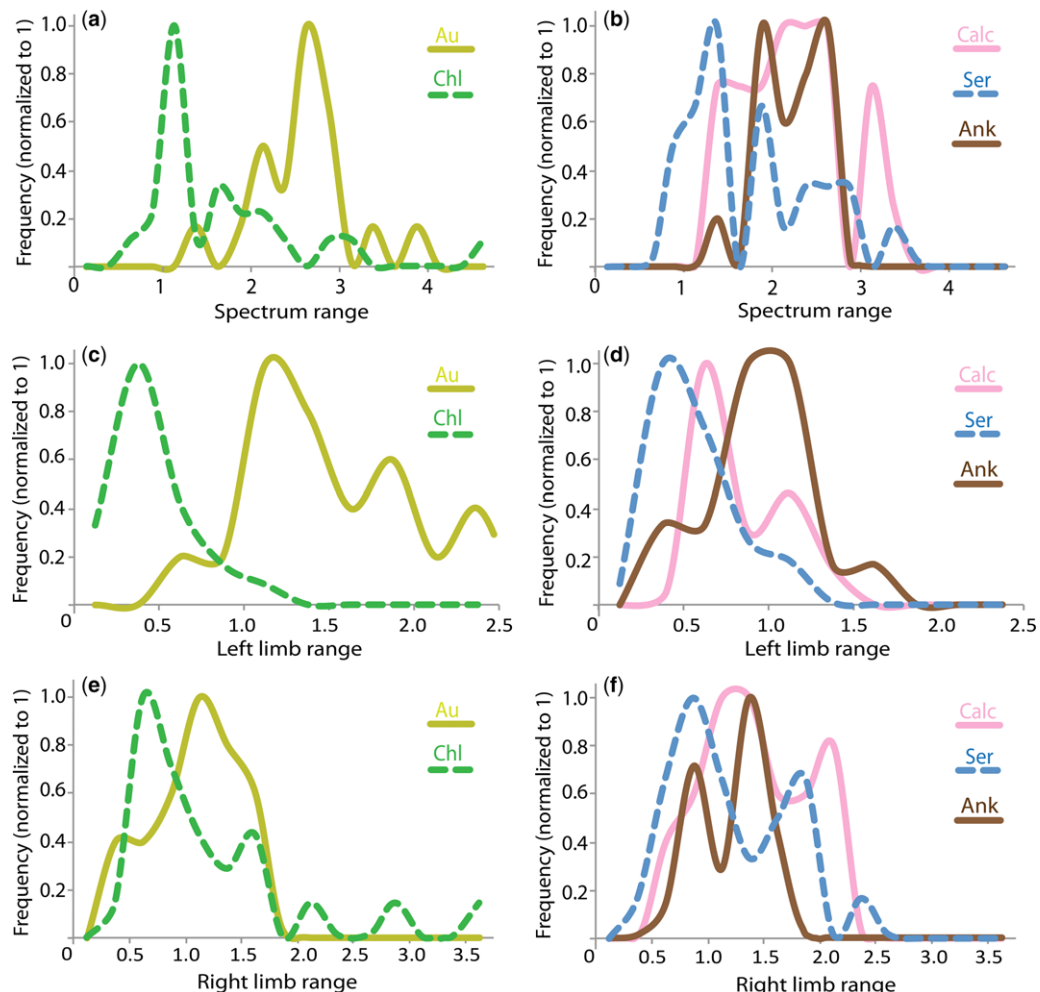


**Fig. 15.** Frequency-normalized histograms of (a, b) singularity spectrum range, (c, d) left limb range and (e, f) right limb range for Au and all mineral phases in Cosmo East. Chlorite has the narrowest singularity spectra of any phase. Sericite also has many narrow spectra. Au has one of the highest modal peaks in the spectrum range. Calcite and ankerite have dominantly intermediate spectrum widths. Sericite and chlorite have the narrowest left-hand limbs; Au has the greatest proportion of broad left-hand limbs. Calcite and ankerite have intermediate left limb widths, with ankerite slightly broader. Sericite and chlorite typically have the narrowest right-hand limbs. Au, calcite and ankerite have strong right-hand limb peaks between 1 and 1.5. Bin width = 0.25. Number of samples: Au, 19; chlorite, 24; sericite, 25; ankerite, 18; and calcite, 25.

proportion of chlorite spectra are weak to moderate ( $\geq 25\%$ ), peaking at c. 32.5%; however, it also has a stronger asymmetry peak at c. 22.5%. With one exception, sericite has exclusively left-handed asymmetry, extending from weak (45%) to strong (10%). It has a strong narrow modal peak of relatively weak asymmetry at c. 37.5%, similar to that in chlorite, and a second of moderate asymmetry at 22.5%. Ankerite shows both left- and right-hand

asymmetry, with the strongest modal peak across the symmetry marker at 50%. It also has a significant proportion of moderate left-handed asymmetry between 25 and 40%. With one exception, calcite also has exclusively left-handed asymmetry, dominated by a strong modal peak of weak asymmetry at 40%. Most of the calcite spectra show similar, but slightly stronger, left-handed asymmetry than ankerite.

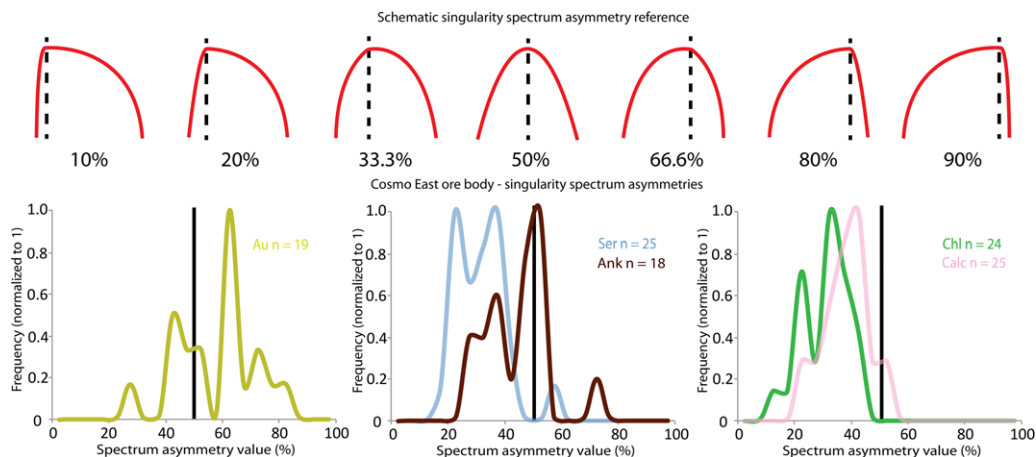


**Fig. 16.** Frequency-normalized histograms of spectrum asymmetry values in Au and all mineral phases in Cosmo East. Reference figure in upper panel shows schematic examples of different asymmetry values. Au shows both left- and right-handed asymmetry. Sericite, chlorite, calcite and ankerite all have almost exclusively left-handed asymmetry. Chlorite and sericite have greater proportions of spectra with stronger asymmetry than calcite and ankerite. Bin width = 5%. n = number of individual drill hole results.

$D_0(\alpha)$ ,  $D_1(\alpha)$ ,  $D_2(\alpha)$ ,  $D_{+\infty}$  and  $D_{-\infty}$  positions for all spectra measured from Cosmo East are provided in Table 5.

In summary, chlorite and sericite in Cosmo East show similar behaviour in many singularity spectrum metrics. Both show the lowest modal peak in the spectrum range of all phases (1–1.25), have the most extreme asymmetries (both almost exclusively left-handed) and the highest  $D_{+\infty}$ ,  $D_1(\alpha)$  and  $D_2(\alpha)$  values. Calcite and ankerite show similar behaviour in spectrum asymmetry (a dominance of symmetry to weakly left-handed asymmetry),  $D_1(\alpha)$ ,  $D_2(\alpha)$  and a dominant modal peak in the spectrum range 2–2.5. However, ankerite has a greater proportion of lower  $D_{+\infty}$  values than calcite

and a narrower variation in spectrum range. Au has a narrow modal peak in spectrum range 2.5–2.75, has the greatest proportion of left-hand asymmetry, the lowest  $D_{+\infty}$  and  $D_2(\alpha)$  values and a bimodal distribution in  $D_1(\alpha)$ .

## Discussion

### Characterization of the non-linear properties of common mineral phases in the Sunrise Dam hydrothermal system

Analysis of Au and five key mineral phases from 207 drillcores (135–1069 m in length) across three

**Table 5.** Singularity spectrum metrics for Au and key mineral phases in Cosmo East (all drillcores)

	No. of samples	$D_0(\alpha)$	$D_1(\alpha)$	$D_2(\alpha)$	$D_{+\infty}$	$D_{-\infty}$
Au	19	1.28–2.43 (1.25–1.5)	0.05–0.96 (0–0.25; 0.75–1)	0.02–0.88 (0–0.25)	0–0.87 (0–0.25)	1.79–3.83 (2.75–3)
Sericite	25	1.14–2.15 (1.25–1.5)	0.71–1.47 (1–1.25)	0.55–1.31 (0.75–1.25)	0.37–1.14 (0.75–1)	1.76–4.11 (1.75–2; 2.25–2.5; 3–3.25)
Chlorite	24	0.97–1.58 (1–1.25)	0.8–1.2 (0.75–1)	0.7–1.17 (0.75–1)	0.57–1 (0.5–1)	1.5–5.18 (1.5–2.25)
Calcite	25	0.9–1.55 (1.25–1.5)	0.38–1.01 (0.5–0.75)	0.19–0.87 (0.25–0.5)	0.04–0.67 (0.25–0.5)	1.62–3.7 (2–2.25; 2.5–2.75)
Ankerite	18	1.02–1.74 (1.25–1.5)	0.33–1.05 (0.5–0.75)	0.15–0.88 (0.25–0.75)	0.06–0.76 (0–0.25)	2.07–3.01 (2–3)

Frequency distribution end-members for each spectrum metric are provided first; numbers in parentheses are the modal peak on the frequency histogram.

## QUANTIFYING HYDROTHERMAL SYSTEMS

texturally distinct ore bodies allowed the characterization of their spatial relation within the Sunrise Dam mineralizing system.

*Chlorite.* Chlorite spectra in each of the three ore bodies share a number of common features:

- (1) almost exclusively left-handed asymmetries (98.5%);
- (2) some of the most extreme spectrum asymmetries of any phase (matched only by sericite); and
- (3) the highest  $D_{+\infty}$ ,  $D_1(\alpha)$  and  $D_2(\alpha)$  values of any phase (matched only by sericite).

Chlorite in the Vogue ore body displays distinct behaviour in hierarchical organization (singularity spectrum range) compared with that in GQ and Cosmo East. Chlorite in GQ and Cosmo East is characterized by a dominance of relatively narrow singularity spectra (typically displaying ranges between 1 and 2), with a lower proportion of spectra with ranges  $>2$ . The low modal peak in Cosmo East is narrower (i.e. shows a stronger preferred spectrum range) than that present in GQ, which is more distributed. These narrow chlorite spectrum ranges in GQ and Cosmo East are lower than all other phases, with the exception of sericite. By contrast, chlorite in Vogue shows a strongly multi-modal distribution in singularity spectrum, with two peaks that are the highest of any phase within the ore body. Therefore, whereas chlorite in GQ and Cosmo East is one of the least hierarchically organized phases, in many parts of Vogue it is the strongest. In other words, chlorite is one of the most regularly distributed phases in GQ and Cosmo East, with relatively consistent amplitudes and wavelengths in both high and low concentrations. Conversely, in many parts of Vogue it is the most irregularly and intermittently distributed phase. Left-handed asymmetry in chlorite from Sunrise Dam indicates that the processes responsible for the spatial distributions of low concentrations (right limb) were more heterogeneous and noisy than those responsible for the distributions of the high concentrations (left limb). The extreme left-handed asymmetries state that relatively strong fluctuations in downhole chlorite concentrations are more common than weaker fluctuations. Having the highest  $D_{+\infty}$ ,  $D_1(\alpha)$  and  $D_2(\alpha)$  values of any phase expresses that the strongest fluctuations in chlorite concentration are generally weaker than the strongest fluctuations in the concentrations of other phases.

*Sericite.* Sericite in each of the three bodies shares a number of common singularity spectrum attributes:

- (1) almost exclusively left-handed asymmetries;
- (2) some of the most extreme spectrum asymmetries of any phase (similar to those of chlorite); and

- (3) the highest  $D_{+\infty}$ ,  $D_1(\alpha)$  and  $D_2(\alpha)$  values of the phases examined (similar to those of chlorite).

Sericite in GQ and Cosmo East show similar hierarchical organization (spectrum ranges) – defined by modal peaks of 0.75–1.25 and 1–1.25, respectively. In both cases these are the lowest modal peaks of any phase, indicating that sericite is the most regularly distributed phase in each ore body – with all concentrations showing relatively uniform spatial behaviour. Geological factors that produce stronger hierarchical organization (greater spectrum ranges) in sericite in a number of GQ and Cosmo East drillcores are discussed in following sections. Sericite in Vogue has one of the most strongly hierarchical organizations of any phase, showing dominantly broad singularity spectrum ranges similar to those of Au. This contrasts with its behaviour in Cosmo East and GQ, where it shows the lowest degree of hierarchical organization. This suggests that sericitic alteration zones in GQ and Cosmo East are more regular in intensity and spacing, but those in Vogue are more heterogeneous and patchy. Left-handed asymmetry in sericite at Sunrise Dam indicates that the processes responsible for the distributions of the common high abundances (left limb) were more uniform than those responsible for the rarer low abundances (right limb).

*Gold.* Au in all three ore bodies shows very similar behaviour in a number of singularity spectrum properties:

- (1) the lowest  $D_1(\alpha)$ ,  $D_2(\alpha)$  and  $D_{+\infty}$  values of all spectra measured;
- (2) highly similar spectrum ranges in each ore body (c. 2–3);
- (3) generally broader singularity spectra than the mineral phases present (with the exception of sericite and chlorite in Vogue); and
- (4) both left- and right-hand asymmetry (weak to moderate).

Examined as entire drillcores at 0.5 m resolution, Au in the GQ, Cosmo East and Vogue ore bodies at Sunrise Dam is not significantly differentiated via the total spectrum, left limb or right limb ranges. The Au spectrum ranges in all three ore bodies mostly lie between 2 and 3, with end-members extending from c. 1 to 4. Within this, Vogue is strongest between 2 and 2.5; Cosmo East and GQ are strongest between 2.5 and 3.

However, importantly, the Au in each ore body shows significant diversity in spectrum asymmetry. It appears that asymmetry is an expression of different processes operating to produce low grades as opposed to high grades. Different processes might, for instance, involve the primary deposition of low grades and dissolution/re-precipitation processes

to form high grades. As such, it appears that similar processes operated to produce both high and low grades in the Vogue and GQ ore bodies (i.e. they have relatively symmetrical spectra), but that different processes operated in the Cosmo deposit (i.e. showing more diverse spectral asymmetries).

*Calcite and ankerite.* Calcite and ankerite in all three ore bodies show similar behaviour in a number of singularity spectrum properties:

- (1) intermediate singularity spectrum ranges, typically between 1 and 3;
- (2) intermediate  $D_1(\alpha)$  and  $D_2(\alpha)$  values; and
- (3) almost exclusively left-hand asymmetry (weak to moderate).

Calcite and ankerite in GQ and Cosmo East show stronger multifractal signatures (i.e. are more irregularly and intermittently distributed) than both host rock alteration minerals associated with mineralization (sericite) and host rock alteration minerals not directly related to mineralization (chlorite). Conversely, calcite and ankerite in Vogue commonly display narrower multifractal signatures (i.e. are more regularly distributed) than sericite and chlorite. Carbonates throughout Sunrise Dam show relatively irregular and intermittent distributions, but are less irregularly distributed than Au.

#### *Geological controls on spatial organization of common mineral phases in hydrothermal systems*

The hierarchical organization of a multifractal is sensitive to the range of relative concentrations in the signal, the relative amplitudes of fluctuations and the wavelengths over which these concentrations correlate. In structurally controlled epigenetic mineral deposits, a number of factors control the distributions of mineralization and associated alteration (and hence their multifractal signatures), including:

- (1) the spatial distribution of host rock types;
- (2) the scales of strain partitioning;
- (3) the deformation style (veining, brecciation, shear zone development);
- (4) the pressure and temperature conditions;
- (5) the fluid composition, including pH; and
- (6) the scales of fluid–rock interaction.

This section examines the influence of dominant host rock type in GQ and Vogue drillcores on the spatial organization of each of the mineral phases. This is followed by discussions of the geological controls on the spatial organization of host rock alteration (sericite and chlorite) and vein and breccia infill carbonates (calcite and ankerite) using specific signal features of key drillcores as

examples. The singularity spectrum ranges for each mineral phase in GQ and Vogue are then compared against those of other phases over the same drillcore intervals to assess the degree to which their spatial organizations are associated with one another.

*Non-linear dynamics of mineral phases classified by dominant host rock type.* Drillholes in GQ and Vogue were classified according to the dominant host rock to evaluate the rock type control on the singularity spectra behaviour. The dominant host rocks in GQ drillcores are andesite, polymictic breccia and conglomerate, and volcaniclastic sandstone. In this section, the host rock classification ‘conglomerate’ is used to encompass both polymictic conglomerate and breccia. Vogue drillcores are almost exclusively andesite-dominated (between 34.6 and 88%), with few exceptions. Vogue drillcores were subdivided into two roughly equal proportions: those where andesite was <65% and those where andesite was ≥65%. The 26 drillcores analysed from Cosmo East subdivided into too many dominant rock types to allow statistically valid comparisons between them. The following section presents the dynamics of mineral phases in Vogue and GQ categorized by the dominant host rock.

Sericite shows similar singularity spectrum ranges in andesite- and conglomerate-dominated sections of GQ, and marginally broader spectra in sections dominated by volcaniclastic sandstone (Fig. 17). Sericite in sections of Vogue composed of lower and higher proportions of andesite both display high proportions of broad singularity spectra with widths between c. 1.5 and 3 (Fig. 18). However, sericite from drillcores in Vogue composed of ≥65% andesite show a greater proportion of narrow spectra with widths between 0.5 and 1.5.

Chlorite in andesite- and conglomerate-dominated sections of GQ shows broad distributions in spectrum range, primarily between 0.5 and c. 3 (Fig. 17). Of the two, the andesite-dominated sections are more evenly distributed across this range. The andesite-dominated sections of GQ have a greater proportion of spectra >3 than the conglomerate-dominated sections. By contrast, chlorite in the sections of GQ dominated by volcaniclastic sandstone shows a dominance of narrow singularity spectra. Chlorite in sections of Vogue dominated by lower and higher proportions of andesite both share two strong peaks at intermediate widths of c. 2 and c. 3 (Fig. 18). However, sections with <65% andesite display a much greater proportion of broad spectra (≥3.5); those with ≥65% andesite display a much greater proportion of narrow spectra (≤1.5).

Calcite in sections of GQ dominated by andesite and volcaniclastic sandstone shows strong

## QUANTIFYING HYDROTHERMAL SYSTEMS

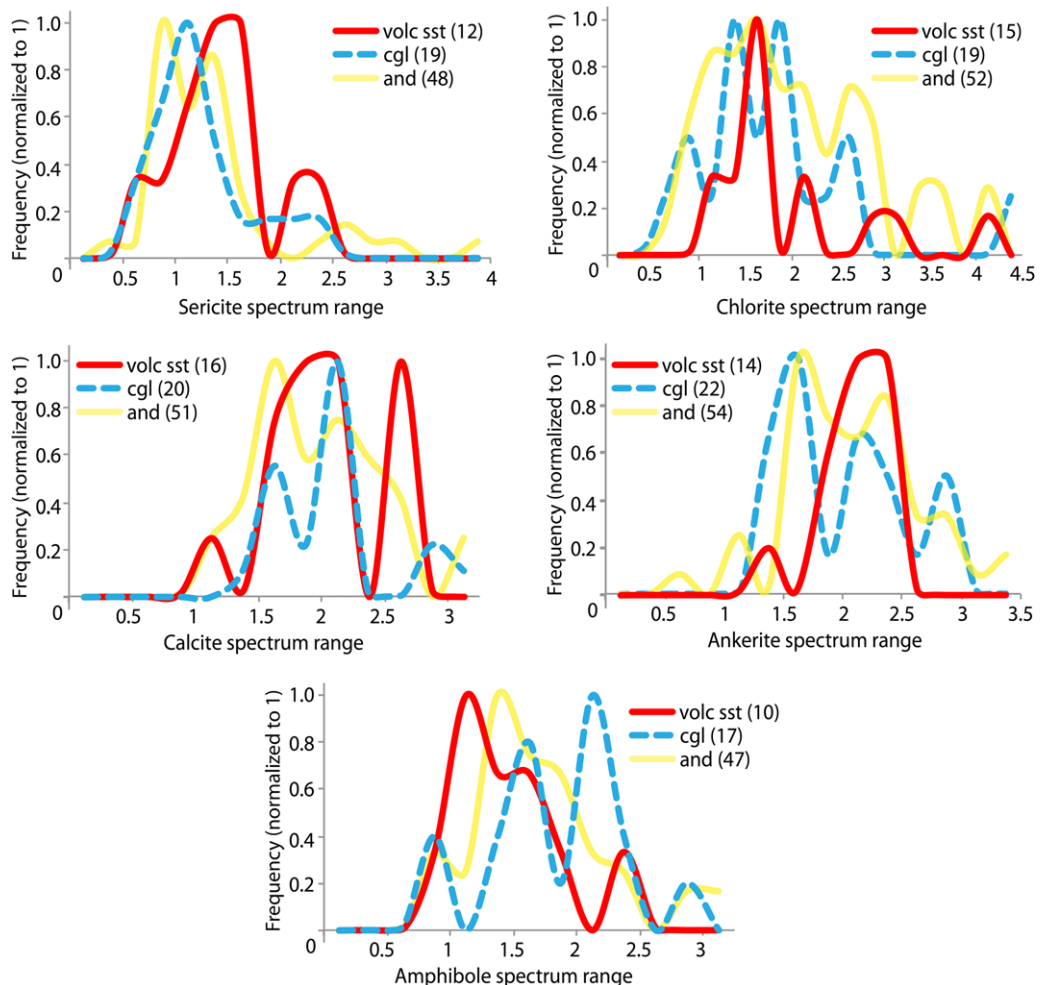


**Fig. 17.** Singularity spectra widths for each phase in GQ classified by the dominant host rock over the drillcore interval: andesite (and), conglomerate (cgl) and volcaniclastic sandstone (volc sst). Each frequency-normalized histogram compares the spectral behaviour of the phase in each of the dominant rock types. The number of singularity spectra used to construct each histogram is shown in brackets. Bin width = 0.25.

variability in singularity spectrum width, between *c.* 1 and 2.75 (Fig. 17). Calcite in sections dominated by volcaniclastic sandstone shows stronger multimodality than that in andesite-dominated sections. Calcite singularity spectra in conglomerate-dominated sections are more consistent (*c.* 1.25–2.25). Calcite singularity spectra in Vogue sections with <65% andesite are marginally broader than in sections with ≥65% andesite (Fig. 18).

Ankerite in andesite- and conglomerate-dominated sections of GQ (Fig. 17) shows strong variability in singularity spectrum width (*c.* 1.5–3.5 and *c.* 1–3, respectively). Conglomerate-dominated sections are more strongly multi-modal than the

andesite-dominated sections. Ankerite singularity spectra in sections of GQ dominated by volcaniclastic sandstone are highly consistent, between *c.* 1.5 and 2.5. Ankerite in Vogue sections with <65% andesite and those with ≥65% andesite both show strong peaks at spectrum widths of *c.* 1.5 (Fig. 18). However, sections with <65% andesite show a greater proportion of broader spectra (an additional peak at 2–2.25).

Amphibole singularity spectra in sections of GQ dominated by andesite and volcaniclastic sandstone show relatively similar distributions, with strong peaks between 1 and 1.5 (Fig. 17). Amphibole in conglomerate-hosted sections of GQ is strongly

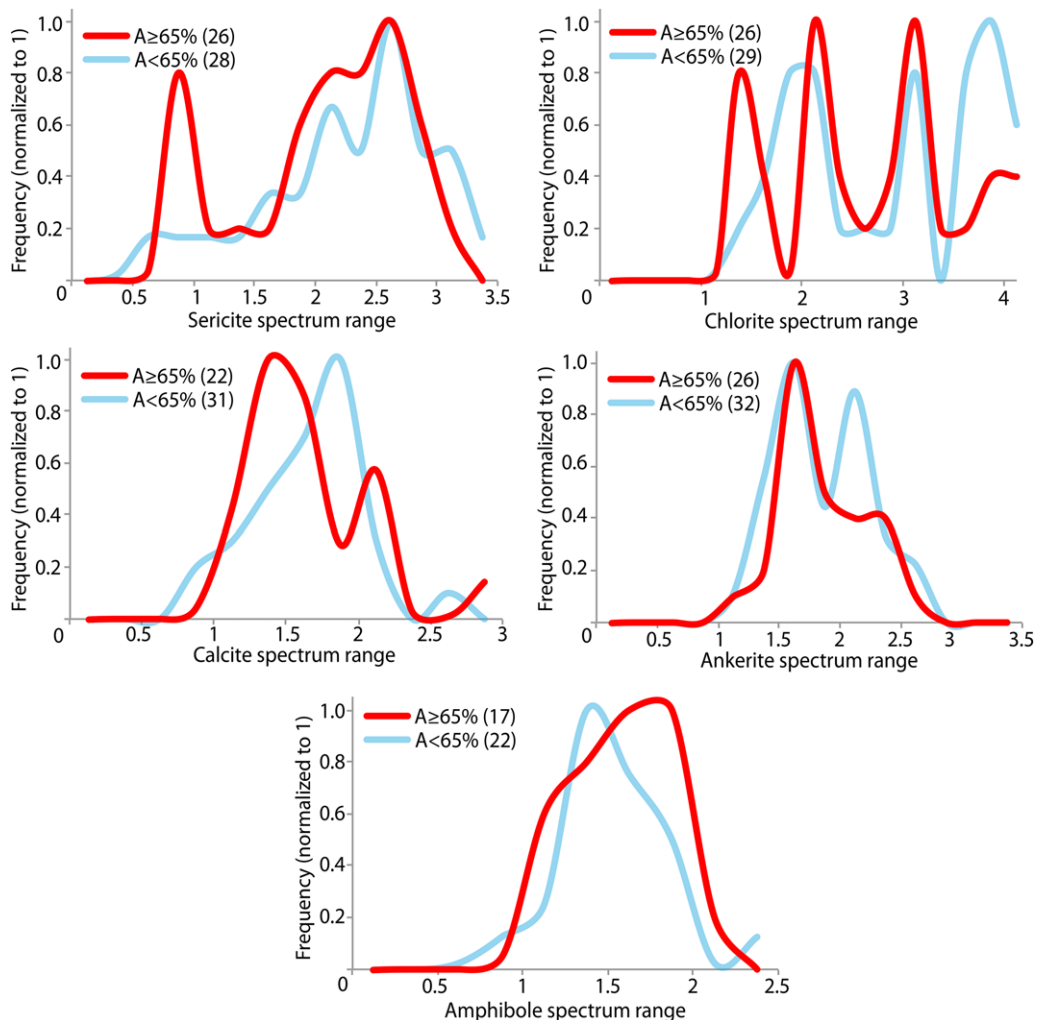


**Fig. 18.** Singularity spectra widths for each phase in Vogue classified by the proportion of the drillcore composed of andesite. Each frequency-normalized histogram compares the behaviour of the phase in Vogue drillcores composed of <65% andesite ( $A < 65\%$ ) v. its behaviour in Vogue drillcores composed of  $\geq 65\%$  andesite ( $A \geq 65\%$ ). The number of singularity spectra used to construct each histogram is shown in brackets. Bin width = 0.25.

multi-modal, with three peaks of increasing strength at c. 0.75, c. 1.5 and c. 2.25. Conglomerate-hosted amphibole in GQ is therefore more strongly multi-fractal than that in sections dominated by andesite and volcaniclastic sandstone. Amphibole singularity spectra in Vogue sections with <65% andesite are generally narrower than those in sections with  $\geq 65\%$  andesite (Fig. 18).

Chlorite spectra in sections of GQ dominated by volcaniclastic sandstone are much narrower than in those dominated by other rock types. Narrow chlorite spectra end-members in Vogue (i.e. those in

which chlorite is more regularly distributed) are more dominant in sections with  $\geq 65\%$  andesite; broad chlorite spectra end-members are more dominant in those with <65% andesite.

In summary, chlorite has more consistent (and narrow) singularity spectra in sections of GQ dominated by volcaniclastic sandstone than in other host rocks. On the other hand, sericite in GQ shows no appreciable variation in spatial dynamics between the three host rocks. Sericite in Vogue displays strong irregularity and intermittency in most of the sections composed of low and high

## QUANTIFYING HYDROTHERMAL SYSTEMS

proportions of andesite. However, sericite is more regularly distributed in a greater proportion of drillcores characterized by  $\geq 65\%$  andesite. Ankerite in sections of GQ dominated by volcanoclastic sandstone is typically more irregular and intermittent than in those dominated by andesite and conglomerate. Calcite is more intermittent and irregularly distributed in Vogue drillcores with  $< 65\%$  andesite than in those with  $\geq 65\%$  andesite. A degree of variation in the spatial behaviour of certain phases can therefore be correlated with the dominant host rock type. However, the following section uses key examples of sericite and chlorite to demonstrate that variations in the spatial dynamics of mineral phases are often strongly controlled by specific rock types that compose minor proportions of a drillcore interval.

*Controls on the spatial organization of sericite and chlorite.* Where sericite and chlorite display narrow singularity spectra, the hyperspectral signals are generally continuous and regular, and self-similarity can be straightforwardly recognized over confined ranges of amplitudes and spatial scales. Here, protolith distributions (host rock compositions), strain partitioning, fluid pathway distributions, fluid availability and scales of fluid–rock reaction have interacted to produce similar variations in the intensity and spatial wavelengths of sericitic and chloritic metasomatism within the system (the latter largely unrelated to primary mineralization). Sericite and chlorite in drillcores defined by narrow singularity spectra commonly show two dominant modal concentration ranges – either very high (of the order of 8000–10 000 counts) or low (in the order of 0–2000), with relatively few intermediate values (e.g. Fig. 19a, b). The high concentration band often dominates and the intervals are characterized by high-amplitude fluctuations between the two bands over wavelengths of the order of a few metres.

On the other hand, in sections of the ore bodies where sericite and chlorite are quantified by a broad singularity spectrum range, this is commonly associated with one of two signal features:

- (1) the presence of at least one strong, relatively sharp, discontinuity in phase concentration (e.g. Fig. 19c); or
- (2) the signal is dominated by (atypically) low concentrations of the phase, punctuated by spatially localized zones of moderate or intense concentrations that correlate at greater wavelengths than the background concentrations (e.g. Fig. 19d).

Both these types of feature increase the number of concentration tiers – enhancing the signal's hierarchical organization. Strong discontinuities in

sericite and chlorite concentration in GQ and Cosmo East are most commonly associated with a dramatic decrease in concentration relative to the rest of the signal. Importantly, sericite and chlorite concentrations in the discontinuities are severely reduced, not entirely eliminated. The significance of this is illustrated later in this paper.

In a number of GQ drillcores (e.g. Fig. 19c), low sericite concentration discontinuities correspond to basalt host rocks. In others, they correspond to volcanoclastic sandstone. Strong concentrations of calcite and ankerite infills in many of these basalt intervals record fluid pathway generation and fluid availability in this part of the system. This indicates that the basalt host rock exerted a chemical control on the sites of sericite-forming reactions, as opposed to a rheologically controlled absence of fluid pathways (i.e. a lack of fracturing and brecciation). Strong sericite concentration discontinuities in other drillcores do not correspond with host rock contacts. Instead, they may reflect differential fluid pathway generation and scales of fluid–rock interaction.

Deconstruction of the sericite discontinuity example in Figure 19c into component intervals for independent analysis (Fig. 20) demonstrates how each component contributes to the singularity spectrum. Figure 20b shows the detail of the sericite signal across the c. 30 m wide basalt interval (92–120 m), where concentrations are  $\leq 25$  counts. Reducing all concentrations in the basalt interval to 0 and reanalysing the entire drillcore (0–142 m) reduces the singularity spectrum range from 3.82 to 0.99 (Fig. 20c). The reduction in spectrum range is almost entirely from the right-hand limb, from 2.91 to 0.43. The left limb remains largely intact (0.91–0.56) and maintains its position on the spectrum plot. Following the removal of the low sericite concentrations in the basalt, a small range of fractal dimensions characterizes the rest of the signal. The spectrum limbs are close together because the high and low probability grades in the remaining signal now scale similarly over a restricted range of amplitudes and wavelengths. The basalt discontinuity therefore strongly influences the multifractal signature of the drillcore. The low concentrations removed from the basalt interval represent the less frequent (low probability) concentrations in the signal. This example demonstrates that the right limb of the spectrum describes the low end-member concentrations in sericite and the left limb describes the high concentrations (high probability). These high and low probability classifications apply to most of the sericite and chlorite signals in Sunrise Dam, unless they are similar to that in Figure 19d, in which low concentrations dominate. This contrasts with typical Au assay signals, in which the rare high Au grades are the lowest

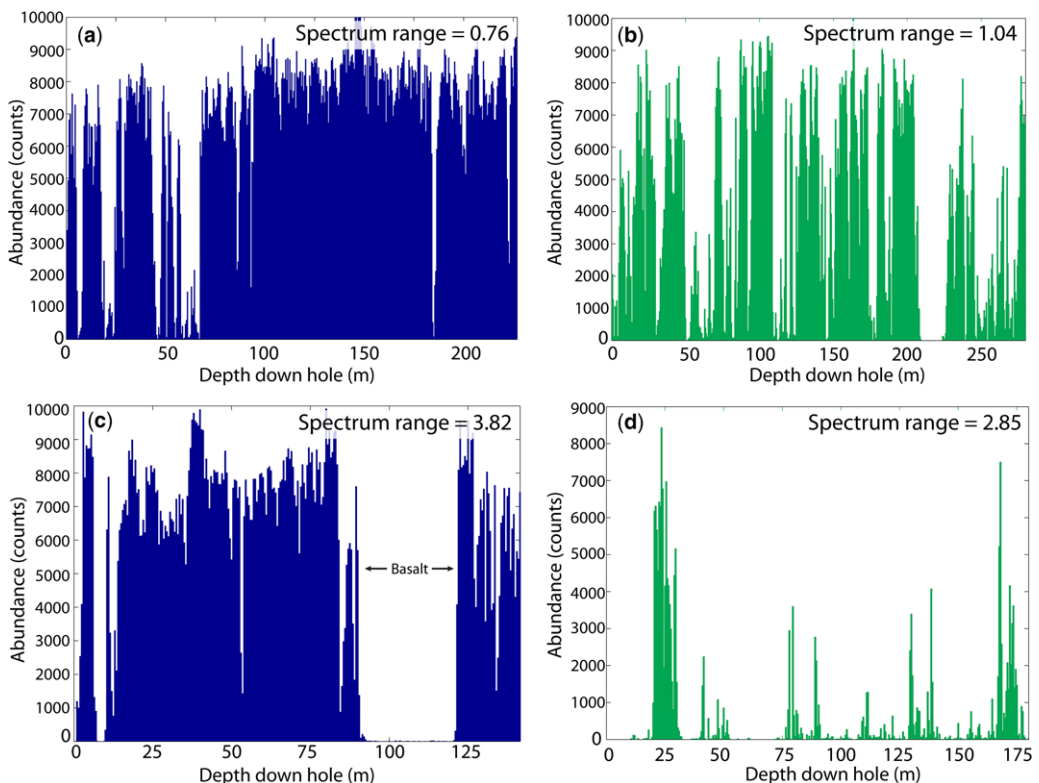


**Fig. 19.** Common types of sericite and chlorite concentration signal at Sunrise Dam, determined by hyperspectral analysis. (a) Sericite signal showing a dominance of high concentrations along the drillcore (*c.* 7000–9000 counts) with high-amplitude fluctuations to less abundant low concentrations (*c.* 0–2000 counts). (b) Chlorite signal with large fluctuations between low and high concentrations over similar wavelengths of up to *c.* 20 m. Proportions of high and low concentrations are roughly equal. (c) Sericite signal with similar behaviour to part (a), but with a strong, sharp *c.* 25 m wide discontinuity. Note that sericite concentrations across the discontinuity (basalt) are extremely low (0–30 counts). The detail of sericite concentration across the basalt unit is shown in Figure 20b. (d) Chlorite signal characterized by atypically low background concentrations of up to *c.* 10 000 counts, punctuated by narrow zones of high abundances similar to the background levels in parts (a), (b) and (c). Variations in signal types (a) and (b) are associated with narrow singularity spectra in sericite and chlorite. The singularity spectrum width for each hole is noted next to the signal. Signal features such as those in parts (c) and (d) are commonly associated with broad singularity spectra. All four signal types are applicable to both phases.

probability and occupy the right limb of the spectrum. In Au assay signals, the relative probabilities shown by high and low concentrations are inverted relative to those in sericite and chlorite.

Analysed independently, sections 1 and 2 in Figure 20a each produce singularity spectra identical to that when the two form a composite signal separated by the 30 m discontinuity devoid of sericite. Importantly, this illustrates that when two multifractals described by the same range of fractal dimensions are amalgamated, the resultant singularity spectrum may remain the same. Geologically, this signifies that structural discontinuities or host rock contacts where a phase is entirely absent may exert no impact on the singularity spectrum.

Low chlorite concentration discontinuities in a number of drillcores from GQ correspond with quartz–feldspar porphyries. Figure 21 demonstrates the influence of one of these quartz–feldspar porphyry intrusions on the multifractal signature of chlorite across the drillcore. The initial chlorite signal in the entire drillcore interval is characterized by a broad singularity spectrum width of 4.15. Removal of low chlorite concentrations across the quartz–feldspar porphyry in Figure 21a results in a dramatic narrowing of the singularity spectrum width to 1.04. The reduction in singularity spectrum is almost entirely from the right limb (low probability, low values) in a similar manner to the sericite example in Figure 20.

## QUANTIFYING HYDROTHERMAL SYSTEMS

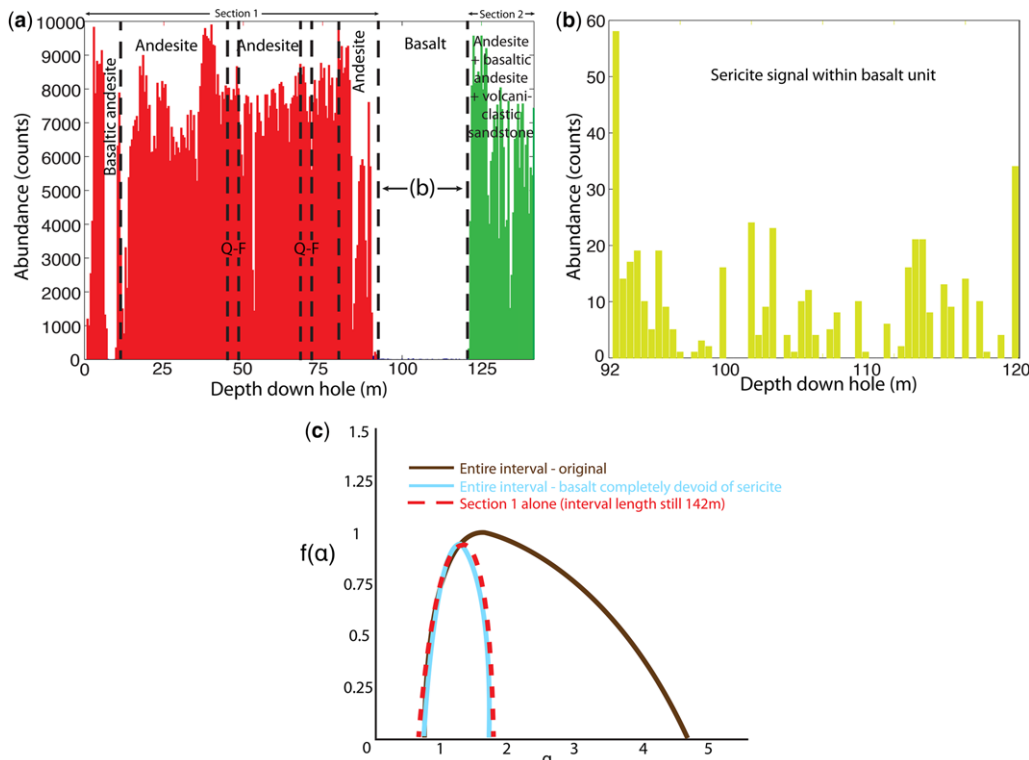


**Fig. 20.** Modification of the sericite signal in Figure 19c to demonstrate the effects of primary rock type contacts and structural discontinuities on the singularity spectrum. (a) Sericite signal from Figure 19c with host rock boundaries marked. Q-F = quartz–feldspar porphyry. The basalt unit corresponds with substantially lower sericite concentrations, the detail of which is shown in (b). Importantly, the sericite concentration in the basalt is dramatically lower, not absent. The portion of the signal to the left of the basalt unit is ‘section 1’; the portion to the right of the basalt is ‘section 2’. The entire original drillcore interval shows a broad singularity spectrum (c; broader spectrum with solid line). All low sericite concentrations across the basalt unit were reduced to 0 and the entire 0–142 m signal re-analysed (maintaining the rest of the signal). When the basalt is devoid of sericite, the singularity spectrum for the drillcore narrows dramatically (narrow spectrum with solid line) demonstrating the strong control of host rock discontinuities on the sericite singularity spectra. This reduction in span is almost entirely from the right-hand limb. When analysed independently (maintaining signal length) section 1 shows an almost identical singularity spectrum to that when the basalt is devoid of sericite (spectrum with dashed line). Therefore discontinuities with reduced concentrations of a phase will increase the spectrum width; those entirely devoid of a phase may not influence the spectrum. Spectrum width may also be increased in discontinuities with significantly increased concentrations of a phase.

Intrusion of the quartz–feldspar porphyry has imposed a strong control on the spatial distribution of chlorite-forming reactions during alteration, increasing the intermittency and irregularity of the signal. Protolith distribution in Sunrise Dam is therefore a first-order control on chlorite multi-fractality (and also sericite). When sections 1 (left) and 2 (right) to either side of the quartz–feldspar porphyry are analysed independently (maintaining the total drillhole length of 210 m), they also display narrow spectrum ranges (0.73 and 1.74, respectively). A low range of fractal dimensions therefore characterizes the scaling dynamics of each individual section.

*Controls on the dynamics of carbonate-forming processes (calcite and ankerite).* Carbonates at Sunrise Dam have been interpreted to be entirely secondary, associated with vein and breccia infill, and wall rock alteration. Their hyperspectral spatial distributions therefore provide a record of carbonate-forming processes associated with alteration in the system. Calcite and ankerite in GQ and Cosmo East have a stronger hierarchical spatial organization than sericite and chlorite, correlating over a large range of wavelengths and amplitudes. Conversely, calcite and ankerite in Vogue are more regular than sericite and chlorite, correlating over a more restricted range of wavelengths and amplitudes.

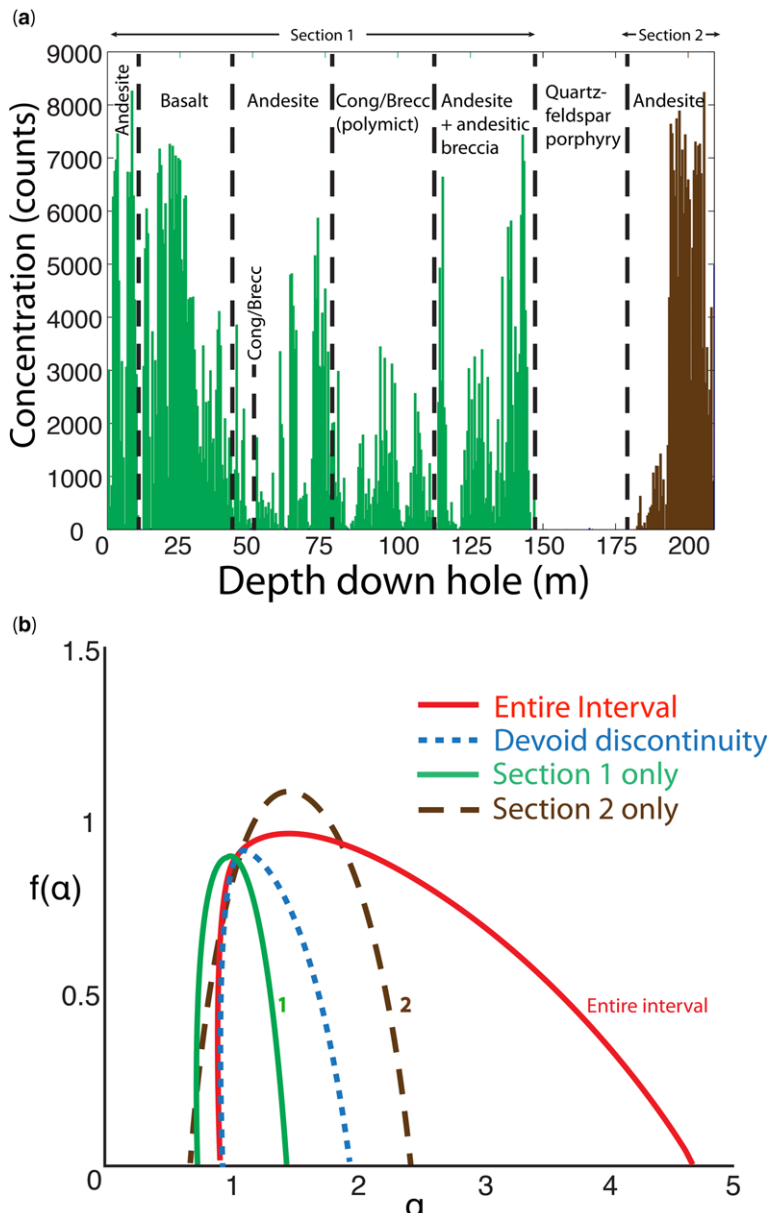


**Fig. 21.** Analysis of different components of a chlorite concentration signal to demonstrate the effects of discontinuities on the singularity spectrum. **(a)** Chlorite signal with host rock boundaries marked. Chlorite concentrations within the quartz–feldspar porphyry unit are sparse and dramatically lower than the surrounding signal ( $\leq 22$  counts). The portion of the signal to the left of the quartz–feldspar porphyry is ‘section 1’; the portion to the right of the quartz–feldspar porphyry is ‘section 2’. The entire original drillcore interval shows a broad singularity spectrum **(b; entire interval)**. All low chlorite concentrations across the quartz–feldspar porphyry unit were reduced to 0 and the signal re-analysed, maintaining the rest of the signal. When the quartz–feldspar porphyry is devoid of chlorite, the singularity spectrum for the entire drillcore narrows dramatically **(b; narrow dashed line spectrum)**. The left limb position of the spectrum is constant. This demonstrates that the low concentration quartz–feldspar discontinuity strongly controls the singularity spectrum. Independently, ‘section 1’ shows a narrow spectrum (spectrum ‘1’); ‘section 2’ a spectrum of moderate width (spectrum ‘2’).

## QUANTIFYING HYDROTHERMAL SYSTEMS

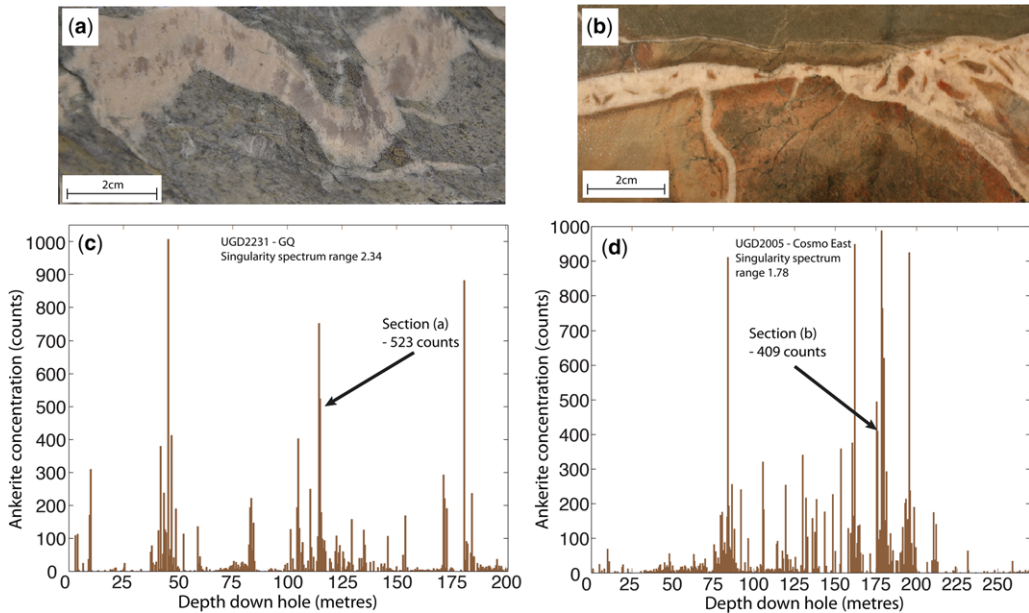


**Fig. 22.** Examples of carbonate vein and breccia cement infill textures associated with strongly elevated concentrations of ankerite well above background levels in some of the 0.5 m drillcore increments. (a) Folded ankerite–quartz veining in extensively sericite-altered andesite from GQ. (b) brecciation in sericite-altered siltstone from Cosmo East infilled with ankerite + quartz cement. (c) Downhole ankerite concentration in drillhole UGD2231 from GQ with the position of the 0.5 m increment in which the sample in part (a) is marked. (d) Downhole ankerite concentration in drillhole UGD2005 from Cosmo East with the position of the 0.5 m increment in which the sample in part (b) is marked. The singularity spectrum range for each drillcore is presented on the downhole ankerite concentration plots. Ankerite in UGD2231 has one of the strongest hierarchical organizations in GQ. Carbonate infill textures shown are ankerite + quartz, but are also commonly observed in calcite.

Calcite and ankerite signatures are most commonly composed of low background concentrations with low-wavelength, high-frequency correlations, punctuated locally by medium to high concentrations that correlate over greater wavelengths. The calcite and ankerite signals therefore share a number of similar characteristics with typical Au assay signatures. Lower concentrations in calcite and ankerite are the most abundant (i.e. are higher probability) and are therefore quantified by the left limb of the singularity spectrum. Conversely, the relatively rare medium to high concentrations are lower probability, quantified by the right limb of the spectrum.

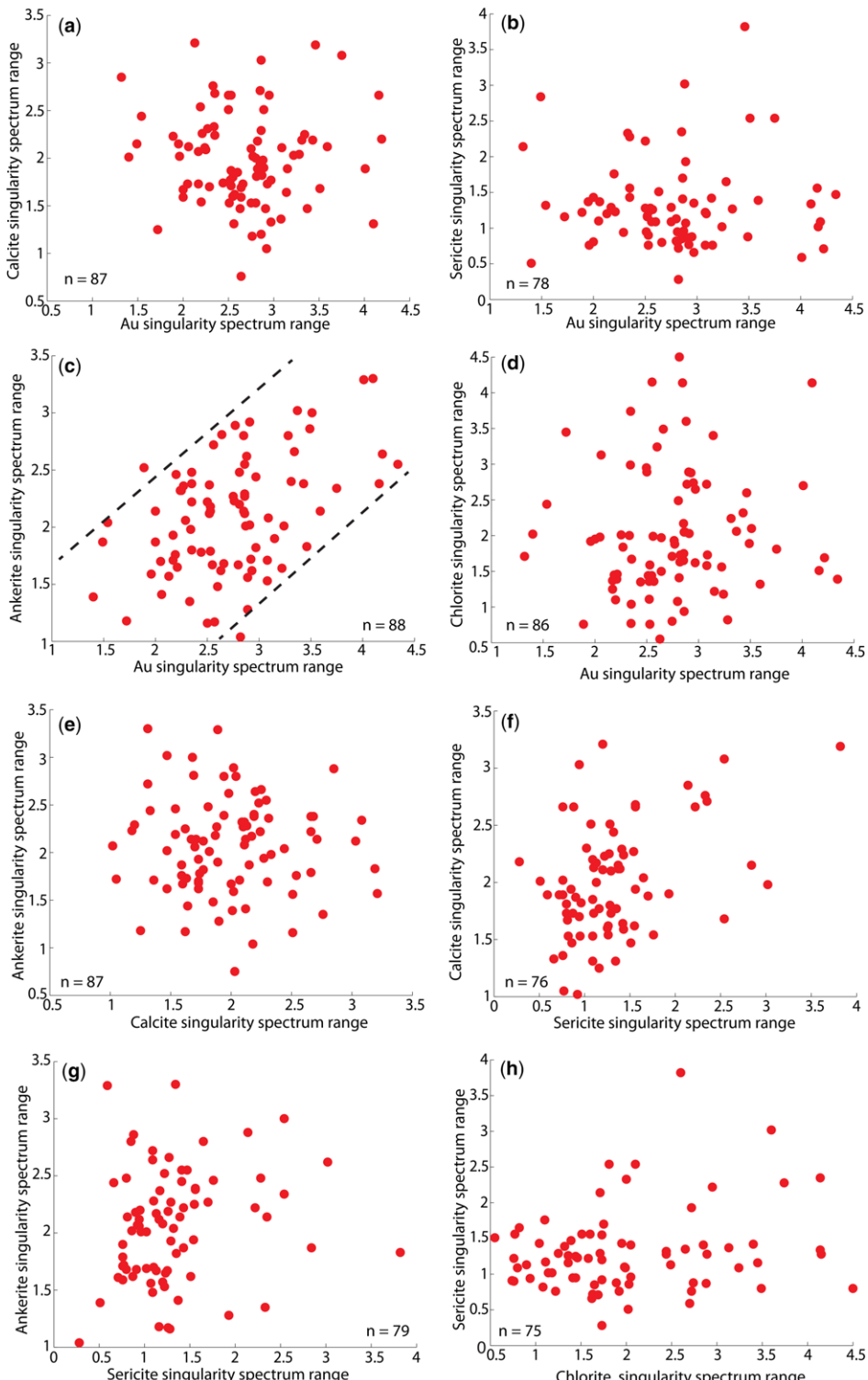
Low background concentrations in carbonate phases will correspond with low volumes of veining, veining dominated by a greater proportion of quartz than carbonate, or minor carbonate involved in host rock alteration. Broader singularity spectra in ankerite and calcite generally correspond to signals with greater contrasts between the common background concentrations and the less frequent medium to high concentrations (higher amplitude fluctuations). Strong contrasts in carbonate concentrations in hydrothermal systems such as Sunrise

Dam are associated with locally high volumes of veining or intense brecciation (e.g. Fig. 22a, b). These localized zones of high concentration infill (e.g. Fig. 22c, d) influence the singularity spectrum by increasing the hierarchical organization of the signal.

Conversely, narrow singularity spectra in calcite and ankerite generally correspond to lower amplitude fluctuations between the low and high concentrations present (i.e. the phase is more regularly distributed throughout the drillhole). More regular amplitudes of fluctuation generally correspond either to drillholes with atypically high background concentrations across the board (e.g. where medium carbonate concentration veining is pervasive throughout) or where sporadic high concentrations (intense veining and/or brecciation) are lacking. The multifractal signature of vein and breccia infill carbonates therefore provides a measure of the regularity of carbonate-bearing veins.

*Comparisons of the dynamics of different phases within individual drillholes.* Figures 23 and 24 show the singularity spectrum range for each

## GQ ore body - singularity spectrum range comparisons



## QUANTIFYING HYDROTHERMAL SYSTEMS

mineral phase against those of other phases over the same drillcore intervals. The Au singularity spectrum ranges in GQ show no correlation with those of calcite, sericite or chlorite (**Figs 23a, b and d**). However, the Au singularity spectrum ranges in GQ do show a positive correlation with ankerite (**Fig. 23c**). Vein-forming phases in GQ (calcite and ankerite) show no correlation in singularity spectrum range (**Fig. 23e**). Sericite and chlorite in GQ also show no correlation in singularity spectrum range (**Fig. 23h**). Calcite and ankerite (vein-forming) show weak positive correlations with host rock alteration (sericite) in most of the drillholes (**Fig. 23f, g**).

The Au singularity spectrum range in Vogue shows no correlation with ankerite, sericite, chlorite and amphibole (**Fig. 24a, c, d, h**). The Au singularity spectrum range does, however, show a moderately positive correlation with calcite (**Fig. 24b**). Sericite (host rock alteration) in Vogue shows a weak positive correlation with calcite (**Fig. 24e**). Ankerite and calcite in Vogue show a positive correlation in the singularity spectrum range (**Fig. 24g**).

The lack of correlation in singularity spectrum width between Au and chlorite in both ore bodies (**Figs 23d & 24d**) is an important observation. This is because petrological interpretations indicate that chlorite host rock alteration at Sunrise Dam is largely unrelated to the primary mineralization (Blenkinsop *et al.* 2007; Roache, pers. comm., 2017). The chlorite abundance locally increases in rocks more distal to mineralization (Blenkinsop *et al.* 2007).

Au and ankerite display a strong positive correlation in singularity spectrum range in GQ (**Fig. 23c**), but no correlation in Vogue (**Fig. 24a**). Therefore Au precipitation is more strongly linked to ankerite-forming reactions in GQ than in Vogue. This suggests that the Au distribution in GQ is more intermittent or nuggety in areas where ankerite precipitation is more irregular and less uniform. The lack of correlation in the singularity spectrum ranges between Au and ankerite in Vogue is comparable with that between Au and chlorite. Conversely, the Au and calcite singularity spectrum ranges display a moderate correlation in Vogue (**Fig. 24b**), but a lack of correlation in GQ (**Fig. 23a**). Au precipitation appears to be more strongly linked to the distribution of calcite-forming reactions in Vogue than in GQ. The lack of correlation

between Au and calcite in GQ is comparable with that between Au and chlorite over the same intervals (which are functions of largely unrelated processes).

Calcite and ankerite show highly similar singularity spectrum metric distributions in both GQ and Vogue. If interpreted on the strength of histogram distributions alone, the two may be naively considered as genetically associated in both ore bodies. However, the differences in spatial dynamics between the two phases are revealed when their spectrum widths for each individual drillcore are compared. This allows distinction of the positive correlation between them in Vogue and a lack of correlation in GQ. The lack of correlation in GQ is consistent with their relative highs and lows commonly being out of phase along drillcores. Phase comparisons within individual drillcores should therefore be integral in the wavelet-based analysis of ore deposits.

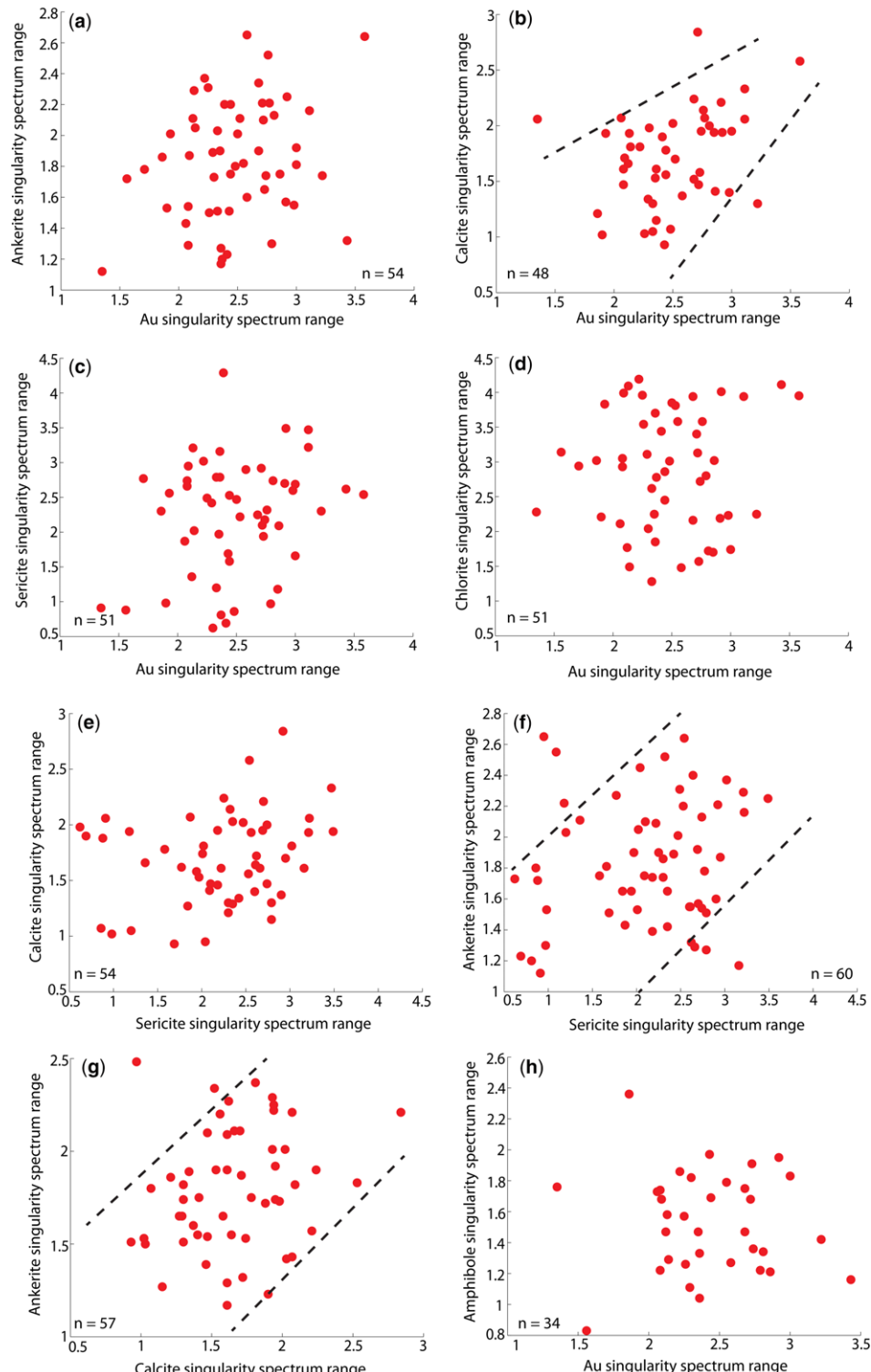
A weak to no correlation exists in the singularity spectrum ranges between the vein-forming mineralogy (calcite and ankerite) and the surrounding host rock alteration (dominantly sericite) in both GQ and Vogue. Texturally, this is a function of the different scales over which each process is manifest. As is common in many hydrothermal systems, veining and brecciation at Sunrise Dam are more spatially confined than the host rock alteration selvages associated with them. Drillcores typically have diameters of c. 5 cm. Therefore a drillcore may intersect a strongly sericitized alteration zone, but miss the proximal fluid conduits in which calcite and ankerite may have crystallized. Alternatively, veining may develop in the absence of host rock alteration, generating a local carbonate peak that does not correspond with sericitic alteration. All of the fluid–rock textures outlined here are manifest at Sunrise Dam. In short, the volume and/or abundance of veining (indicated by the relative carbonate abundance) is not necessarily proportional to the spatial extent of pervasive alteration in the surrounding host rocks.

The singularity spectrum that quantifies a mineral phase or element is sensitive to its downhole spatial organization in peaks and troughs and the relative concentration at each downhole increment. Therefore, if the signals of two mineral phases are identical with respect to both of these criteria, then

---

**Fig. 23.** Scatter plots comparing the widths of singularity spectra between different phases over the same drillcore intervals in the GQ ore body. Au shows a lack of correlation with calcite (**a**), sericite (**b**) and chlorite (**d**). However, it shows a corridor of positive correlation in spectrum width with ankerite (**c**) (marked), indicating that the multiplicative processes responsible for their spatial distributions are linked. The correlation between Au and ankerite in the GQ ore body is stronger than that between them in the Vogue ore body (**Fig. 24**). The vein and breccia cement-forming carbonates (calcite and ankerite) show a lack of correlation (**e**). Calcite and ankerite (vein-forming) show weak positive correlations with host rock alteration (sericite) in most of the drillholes (**f, g**). Chlorite and sericite show no correlation (**h**).

## Vogue ore body - singularity spectrum range comparisons



## QUANTIFYING HYDROTHERMAL SYSTEMS

they will produce identical singularity spectra. However, the relative proportions of two phases produced at a given site is dependent on the relative volumes of each reaction product, the reaction kinetics and the availability of the reactants. This is further compounded where the two product phases are locally produced via different reactions. Consequently, two phases with a strong spatial association may start to diverge in spectrum behaviour if the relative strengths of highs and lows vary between the two. This type of relationship may explain why the positive correlation in spectrum range between Au and ankerite in GQ forms a corridor with a degree of freedom (Figs 23 & 24).

Divergence in singularity spectrum behaviour between two genetically associated phases or elements may also indicate that one of the two is associated with processes outwith those responsible for the formation of the other. For example, every occurrence of Au in a drillhole, or ore body, may be hosted in ankerite veining. However, a proportion of ankerite veins in the system may also be devoid of Au, producing different spatial organizations in ankerite and Au. Therefore although Au is genetically associated with ankerite, they may have different spectra. This may be further complicated when Au mineralization is associated with more than one generation of veining. The first episode of Au mineralization may show a strong association with ankerite-only veins. A second phase of Au mineralization may be associated with calcite-only or quartz-only veins, diluting the initial spatial association with ankerite.

Au precipitation may also be preferentially associated with reactions producing one specific compositional end-member of a phase. This occurs in parts of GQ, where Au is spatially associated with paragonite compositional members of sericite. However, these relationships may be masked where the phase abundances are aggregates of all compositional end-members (that is, the entire hyperspectral wavelength absorption range displayed by the phase). Au and associated phases are not expected to display perfectly linear (1:1) correlations in singularity spectrum metrics because the relative strength of the concentration maxima between their signals will always show a degree of variation. A comparison of the spatial organization in Au abundance with that of independent compositional

members of sericite would be a useful way of quantifying and evaluating genetic links. This represents an important future application of wavelet analysis.

Importantly, spatial organization in calcite, ankerite, sericite and chlorite throughout Sunrise Dam shows almost exclusively left-handed asymmetry (Figs 12, 14 & 16). This describes more complex behaviour in the rare concentrations of infill carbonates and wall rock alteration in the system and relatively uniform behaviour in the common concentrations. This suggests that the processes operating to produce typical concentrations of alteration and infill mineralogy during the lifetime of the hydrothermal system were different from those that produced the rare concentrations in each.

#### *Long-range correlations in gold and key mineralogy at Sunrise Dam*

Hurst exponent analysis was conducted on the downhole abundance of Au and a suite of minerals (chlorite, sericite, calcite and ankerite) for four drillholes, two from GQ (UGD 2232 and UGD 792) and two from Vogue (UGD 2060 and UGD 2418). UGD 2232 and UGD 792 were selected from GQ because they show very different singularity spectral signatures in Au and mineral phases. Au, sericite and calcite from UGD 2232 show very broad singularity spectrum ranges (3.46, 3.82 and 3.19, respectively), whereas in UGD 792 they show significantly narrower spectrum ranges (2.35, 2.28 and 2.1, respectively). UGD 2060 and UGD 2418 were selected from Vogue because they show end-member singularity spectrum ranges in sericite (3.49 and 0.69, respectively), both have some of the broadest spectra in chlorite (4.01 and 3.44, respectively) and significantly different spectra in ankerite (2.25 and 1.23, respectively).

Hurst exponents ( $H$ ) were calculated for every progressive increase in wavelet size (i.e. one voice increments) starting at a minimum of eight voices (0.5 m; the resolution of the dataset).

Figure 25 shows the behaviour of  $H$  with increasing examination (wavelet) scale for Au and a suite of key mineralogy (sericite, chlorite, calcite and ankerite) in the four drillholes. The values of  $H$  for all minerals in each drillcore extend up to and converge at c. 0.85–0.95 at the largest scales of examination.

**Fig. 24.** Scatter plots comparing the widths of singularity spectra between different phases over the same drillcore intervals in the Vogue ore body. Au shows a lack of correlation with ankerite, sericite and chlorite (**a, c, d**). However, the majority of Au v. calcite data show a moderate positive correlation (**b**). The relationship between Au and ankerite in the Vogue ore body is weaker than that in the GQ ore body (Fig. 23c). Calcite and ankerite in Vogue show a corridor of positive correlation in singularity spectrum width (**g**). This relationship is stronger than that between them in the GQ ore body (Fig. 23e). Calcite and ankerite (vein-forming) show weak positive correlations with host rock alteration (sericite) in most of the drillholes (**e, f**). Dashed lines indicate corridors of correlation defined by most of the points in a plot.

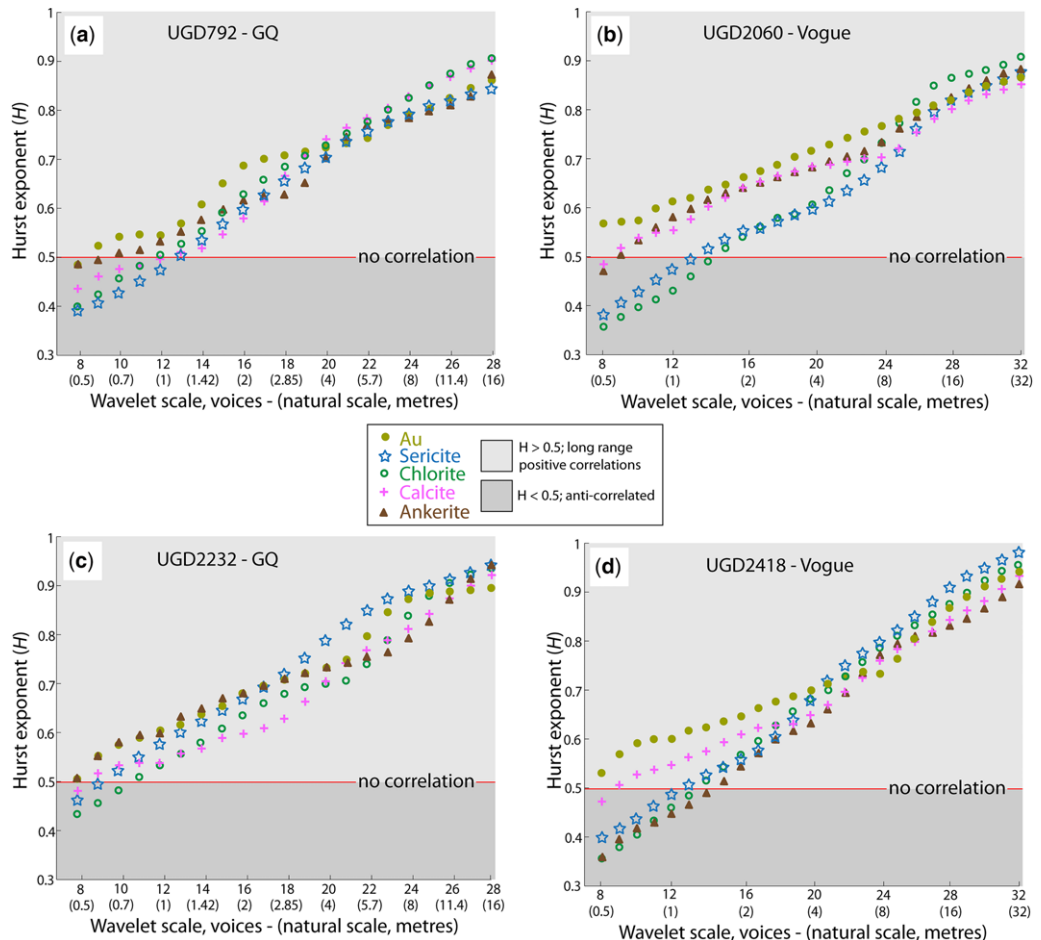


**Fig. 25.** Comparisons of Hurst exponent ( $H$ ) behaviour with increasing wavelet scale for Au, chlorite, sericite, calcite and ankerite in four drillcores from Sunrise Dam. (a) UGD792 and (c) UGD2232 are from the GQ ore body; (b) UGD2060 and (d) UGD2418 are from the Vogue ore body.  $H$  values are presented for wavelet scales of eight voices (0.5 m; the resolution of the dataset) to the maximum wavelet size applied (parts (a, c), 28 voices; parts (b, d), 32 voices). The scale of onset of long-range positive correlations for each phase is marked by a significant rate of increase in  $H$  and  $H \geq 0.5$ . Long-range correlations in sericitic and chloritic host rock alteration (related to and largely not related to mineralization, respectively) are generally present at larger scales than in primary mineralization (Au) and vein and breccia infill carbonates (calcite and ankerite). The exception to this is ankerite in UGD2418 (d).

At the smallest scale of examination (eight voices), Au in the four drillholes has the highest values of  $H$  of all phases, matched by ankerite in UGD792 and UGD2232. This expresses that Au signals have the lowest degrees of roughness at this scale. At the same scale, sericite and chlorite consistently have the lowest values of  $H$  (matched by ankerite in UGD2418) and calcite has intermediate values of  $H$ . This expresses that chlorite and sericite have the highest degrees of roughness at this scale. Geologically, this corresponds to the

observation that typical Au concentrations are more homogeneous across most of the drillcore, whereas those of host rock alteration and vein infill mineralogy fluctuate more extremely and more frequently. Au in each of the drillholes has values of  $H$  of *c.* 0.5 or slightly higher at all scales of examination, including the smallest. In UGD2232 and UGD2418, sharp rates of increase in Au  $H$  between eight and nine voices mark the onset of long-range correlations at scales between *c.* 0.5 and 0.6 m. In UGD792 and UGD2060, sharp rates of increase in

## QUANTIFYING HYDROTHERMAL SYSTEMS

Au  $H$  at *c.* 13 and *c.* 10 voices, respectively, mark the onset of long-range correlations at scales of *c.* 1.2 and *c.* 0.7 m. These scales of long-range correlation in Au (*c.* 0.5–0.7 m and greater) are consistent with the example presented by Ord *et al.* (2016).

Sericite and chlorite share similar  $H$  trajectories in each drillcore. Long-range correlations in chlorite and sericite generally commence at scales larger than those of other minerals, with the exception of calcite in UGD792 and ankerite in UGD2418. In UGD792, UGD2060 and UGD2418 (Fig. 25a, b and d, respectively), long-range positive correlations in both chlorite and sericite occur at similar wavelet scales of *c.* 12–14.5 (1–1.5 m). In UGD792, long-range positive correlations in chlorite and sericite commence at slightly smaller scales of 11 and 9 voices (*c.* 0.85 and *c.* 0.6 m), respectively. In three of the four drillcores, long-range positive correlations in chlorite commence at marginally larger scales than sericite.

Long-range positive correlations in calcite commence at scales intermediate to those of Au (lower) and sericite and chlorite (higher) in three of the drillcores (UGD2060, UGD2232 and UGD2418). In these cases, long-range positive correlations in calcite occur at about the same scales (8.5, 8.5 and 9 voices, respectively; *c.* 0.55–0.6 m). However, long-range positive correlations in calcite in UGD792 occur at a larger scale (14 voices; 1.42 m), similar to that of sericite. Long-range positive correlations in ankerite commence at scales of 11, 9 and 8.5 voices (*c.* 0.85, *c.* 0.6 and *c.* 0.55 m) in UGD792, UGD2060 and UGD2232, respectively. In UGD2060 and UGD2232, this behaviour is similar to calcite (i.e. long-range positive correlations in the two dominant vein and breccia cement-forming phases occur at highly similar scales). In UGD792, long-range correlations in ankerite occur at a smaller scale (11 voices; *c.* 0.85 m) than in calcite (14 voices; *c.* 1.42 m). In UGD2418, long-range correlations in ankerite occur at a larger scale than all other minerals (14.5 voices; *c.* 1.56 m) and its counterparts in other drillholes. This is significantly higher than the other vein-forming carbonate, calcite (nine voices; 0.6 m).

In the examples examined, long-range positive correlations in mineralization (Au) most commonly occur at scales of 0.5–0.7 m and greater, with one exception at *c.* 1.2 m. Long-range positive correlations in host rock alteration (sericite) occur at scales of *c.* 1–1.25 m and greater (including the example presented by Ord *et al.* 2016), with one exception at *c.* 0.6 m. This is similar to chlorite (host rock alteration not directly associated with primary mineralization), in which long-range positive correlations occur at scales of 0.85–1.56 m and greater (including the example in Ord *et al.* 2016).

Long-range correlations in the vein and breccia cement-forming carbonates (calcite and ankerite) typically occur at similar scales of 0.55–0.65 m (ankerite) and 0.55–0.85 m (calcite). However, in UGD2418, the behaviour of the two diverge significantly, with long-range correlations in calcite commencing at significantly smaller scales (*c.* 0.55 m) than ankerite (*c.* 1.56 m).

Scales of long-range correlation onset in primary Au mineralization are similar to those of most of vein and breccia infill carbonates. Long-range correlations in the mineralization-related host rock alteration (sericite) and largely unrelated alteration (chlorite) typically occur at larger scales than in Au or the vein and breccia-forming carbonates. Future work will see the automation of the analysis of  $H$  and its application to large numbers of Au and mineral phase datasets from Sunrise Dam and other deposits. This will facilitate characterization of the scales of long-range correlations between individual ore bodies.

## Conclusions

Hyperspectral reflectance imaging is a fundamental exploration tool routinely utilized to evaluate spatial distributions in the abundance and composition of mineralogy in a wide range of ore deposits. We used wavelet analysis of conventional hyperspectral logs of drillcore from the well-endowed Sunrise Dam hydrothermal system of Western Australia to demonstrate quantitatively that Au, common vein-hosted mineralogy (calcite and ankerite), host rock alteration related to mineralization (sericite) and host rock alteration largely unrelated to mineralization (chlorite) organize spatially as multifractals. We showed that the wavelet-based quantification of hyperspectral reflectance signals is an important tool in ore deposit analysis, complementing core and thin section based petrological and structural investigations. The multifractal organization documented in this deposit is sufficient to show that the spatial organization of Au and alteration mineral assemblages is the result of underlying deterministic dynamic processes rather than the result of random stochastic processes. These results serve as both a confirmation and an elaboration of an increasing body of evidence documenting the fractal nature of geological and mineralizing processes.

The degree to which the multifractal signatures (spectrum range) of two mineral phases or elements in an ore body align with one another may be utilized as a measure of the degree to which the processes responsible for their spatial organization are linked. This is demonstrated by a complete lack of correlation between primary Au mineralization and chlorite in all ore bodies, but a moderate to

strong positive correlation between primary Au mineralization and vein-hosted ankerite in the GQ ore body.

Hurst exponent analysis shows that the scales of the onset of long-range correlation in primary Au mineralization are similar to those shown by most vein and breccia infill carbonates (0.5–0.7 and 0.55–0.85 m, respectively). Long-range correlations in sericitic and chloritic host rock alteration typically occur at larger scales (*c.* 1–1.25 and 0.85–1.56 m, respectively). This is important because long-range correlations in Au distributions ( $H \approx 0.9$ ) only become apparent at length scales of *c.* 10–30 m, which is much larger than the scales at which parts of drillcore or mining operations are normally viewed (on the order of *c.* 1–5 m). However, such observations give some clues as to the length scales involved with the processes operating to produce Au grade distributions; such length scales might include those for fluid mixing or be the length scale for interactions between fluids and heat transfer processes. These processes are often poorly or uncorrelated at small spatial scales (on the order of *c.* 1–5 m), but become correlated at larger length scales.

This research has investigated three different ore bodies spatially associated at the camp scale. Many more studies of this type are needed in a variety of different ore bodies with differing endowments to see the emerging patterns and relationships. Although the scales of analysis in this study were at 0.5 m resolution, wavelet analysis may be applied to hyperspectral datasets of any resolution (down to, and including, detailed sub-millimetre scales). Wavelet analysis is also readily applicable to other routinely acquired drillcore datasets, including chemical element abundances, petrophysical data and gamma logs. Future research should carry out wavelet examination of these other datasets, integrating the results with those extracted from hyperspectral data. The wavelet approach outlined in this study is also applicable to a broad range of deposit types beyond the scope of hydrothermal mineral systems.

This project is funded by a grant from the Minerals Resource Institute of Western Australia (MRIWA) – Project: M424, Multiscale Dynamics of Hydrothermal Mineral Systems. We thank AngloGold Ashanti, Silver Lake Resources, First Quantum Minerals Ltd and The Geological Survey of Western Australia for financial support and access to data. We also thank Greg Hall, Julian Vearncombe and Marcus Willson for encouraging us to explore non-linear systems. Tony Roache and Sarah Firth are thanked for detailed discussions regarding the acquisition and use of hyperspectral reflectance data. Sandi Occhipinti, Catherine Spaggiari and Ian Tyler are also thanked for discussions and facilitating access to data. We thank Klaus Gessner, Peter Sorjonen-Ward, Dirk Nieuwland

and June Hill for thorough reviews that substantially improved the content, layout and focus of this paper.

## References

- AGTERBERG, F.P. 1995. Multifractal modeling of the sizes and grades of giant and supergiant deposits. *International Geology Review*, **37**, 1–8.
- ARNEODO, A., BACRY, E. & MUZY, J.F. 1995. The thermodynamics of fractals revisited with wavelets. *Physica A: Statistical Mechanics and its Applications*, **213**, 232–275.
- ARNEODO, A., AUDIT, B., DECOSTER, N., MUZY, J.-F. & VAILLANT, C. 2002. Wavelet based multifractal formalism: applications to DNA sequences, satellite images of cloud structure and stock market data. In: BUNDE, A., KROPP, A. & SCHELLNHUBER, H.J. (eds) *The Science of Disasters: Climate Disruptions, Heart Attacks and Market Crashes*. Springer, Berlin, 26–102.
- ARNEODO, A., AUDIT, B., KESTENER, P. & ROUX, S. 2003. A wavelet-based method for multifractal image analysis: from theoretical concepts to experimental applications. *Advances in Imaging and Electron Physics*, **126**, 1–92.
- AUDIT, B. 2008. The wtmm1d Package. Managing Singularity Spectrum Computation of 1d Data-Series. Last-wave Software wtmm1d Script Reference Manual, [www.cmap.polytechnique.fr/~bacry/ftp/LastWave/Doc/wtmm1d-doc.pdf](http://www.cmap.polytechnique.fr/~bacry/ftp/LastWave/Doc/wtmm1d-doc.pdf)
- BACRY, E. 2009. LastWave 3.0 Reference Manual, [www.cmap.polytechnique.fr/~bacry/LastWave/index.html](http://www.cmap.polytechnique.fr/~bacry/LastWave/index.html)
- BAK, P. 1996. *How Nature Works: the Science of Self-organized Criticality*. Copernicus, Springer, New York.
- BAKER, T., BERTELLI, M., BLENKINSOP, T., CLEVERLEY, J., MCLELLAN, J., NUGUS, M. & GILLEN, D. 2010. P-T-X conditions of fluids in the sunrise Dam Gold deposit, Western Australia, and implications for the interplay between deformation and fluids. *Economic Geology*, **105**, 873–894.
- BECK, C. & SCHLÖGL, F. 1993. *Thermodynamics of Chaotic Systems*. Cambridge University Press, Cambridge.
- BLENKINSOP, T.G. 1994. The fractal dimension of gold deposits: two examples from the Zimbabwe Archaean craton. In: KRÜHL, J.H. (ed.) *Fractal and Dynamic Systems in Geosciences*. Springer, Berlin, 247–258.
- BLENKINSOP, T., BAKER, T., MCLELLAN, J., CLEVERLEY, J. & NUGUS, M. 2007. *Sunrise Dam Gold Mine Geological Study Project*. Final Report, Project G15, pmdCRC <https://data.gov.au/dataset/project-g15-final-report>
- BROWN, S.M., FLETCHER, I.R., STEIN, H.J., SNEE, L.W. & GROVES, D.I. 2002. Geochronological constraints on pre-, syn-, and postmineralization events at the world-class Cleo gold deposit, Eastern Goldfields province, Western Australia. *Economic Geology*, **97**, 541–559.
- CARLSON, C.A. 1991. Spatial distribution of ore deposits. *Geology*, **19**, 111–114.
- CARRANZA, E.J.M. 2009. Controls on mineral deposit occurrence inferred from analysis of their spatial pattern and spatial association with geological features. *Ore Geology Reviews*, **35**, 383–400.

## QUANTIFYING HYDROTHERMAL SYSTEMS

- CHAINAIS, P. 2006. Multidimensional infinitely divisible cascades. *The European Physical Journal B – Condensed Matter and Complex Systems*, **51**, 229–243.
- CHENG, Q.M. 2007. Mapping singularities with stream sediment geochemical data for prediction of undiscovered mineral deposits in Gejiu, Yunnan Province, China. *Ore Geology Reviews*, **32**, 314–324.
- COOPER, R.W., WYCIE, N.L., STRONG, C.A., DAY, L.J., JONES, J.A. & IRIMIES, F. 2017. *Western Australia Atlas of Mineral Deposits and Petroleum Fields 2017* [PDF]. Retrieved from <http://dmpbookshop.eruditetechnologies.com.au/product/western-australia-atlas-of-mineral-deposits-and-petroleum-fields-2017.do>
- CUDAHY, T., HEWSON, R. ET AL. 2009. Drill core logging of plagioclase feldspar composition and other minerals associated with Archaean gold mineralization at Kamalda, Western Australia, using a bidirectional thermal infrared reflectance system. *Reviews in Economic Geology*, **16**, 223–235.
- DUURING, P., HASSAN, L., ZELIC, M. & GESSNER, K. 2016. Geochemical and spectral footprint of metamorphosed and deformed VMS-style mineralization in the Quinns district, Yilgarn Craton, Western Australia. *Economic Geology*, **111**, 1411–1438.
- FEDER, J. 1988. *Fractals*. Plenum, New York.
- FORD, A. & BLENKINSOP, T.G. 2008. Combining fractal analysis of mineral deposit clustering with weights of evidence to evaluate patterns of mineralization: application to copper deposits of the Mount Isa Inlier, NW Queensland, Australia. *Ore Geology Reviews*, **33**, 435–450.
- HANTLER, A. 2009. *Paragenesis of mineralized veins at Sunrise Dam Gold Mine, Laverton, Western Australia*. MSc thesis, Economic Geology Research Unit, James Cook University.
- AYNES, D.W., CROSS, K.C., BILLS, R.T. & REED, M.H. 1995. Olympic Dam ore genesis: a fluid-mixing model. *Economic Geology*, **90**, 281–307.
- HILL, E.J., OLIVER, N.H.S., CLEVERLEY, J.S., NUGUS, M.J., CARSWELL, J. & CLARK, F. 2014. Characterisation and 3D modelling of a nuggety, vein-hosted gold ore body, Sunrise Dam, Western Australia. *Journal of Structural Geology*, **67**, 222–234.
- HOBBS, B.E. & ORD, A. 2015. *Structural Geology: the Mechanics of Deforming Metamorphic Rocks*. Elsevier, Amsterdam.
- HOBBS, B.E., ORD, A., ARCHIBALD, N.J., WALSHE, J.L., ZHANG, Y., BROWN, M. & ZHAO, C. 2000. Geodynamic modelling as an exploration tool. In: *After 2000 – The Future of Mining*. Australasian Institute of Mining and Metallurgy, Sydney, 34–49.
- HOLLIS, S.P., YEATS, C.J. ET AL. 2015. A review of volcanic-hosted massive sulfide (VHMS) mineralization in the Archaean Yilgarn Craton, Western Australia: tectonic, stratigraphic and geochemical associations. *Precambrian Research*, **260**, 113–135.
- INGEBRITSEN, S.E., GEIGER, S., HURWITZ, S. & DRIESNER, T. 2010. Numerical simulation of magmatic hydrothermal systems. *Reviews of Geophysics*, **48**, RG1002.
- JONES, S., HERRMANN, W. & GEMMEL, J.B. 2005. Short Wavelength Infrared Spectral Characteristics of the HW Horizon: Implications for Exploration in the Myra Falls Volcanic-Hosted Massive Sulfide Camp, Vancouver Island, British Columbia, Canada. *Economic Geology*, **100**, 273–294.
- KUMAR, P. & FOUFOULA-GEORGIOU, E. 1997. Wavelet analysis for geophysical applications. *Reviews of Geophysics*, **35**, 385–412.
- LAUKAMP, C., SALAMA, W. & GONZÁLEZ-ÁLVAREZ, I. 2016. Proximal and remote spectroscopic characterisation of regolith in the Albany–Fraser Orogen (Western Australia). *Ore Geology Reviews*, **73**, 540–554.
- LESTER, D.R., ORD, A. & HOBBS, B.E. 2012. The mechanics of hydrothermal systems: II. Fluid mixing and chemical reactions. *Ore Geology Reviews*, **49**, 45–71.
- LIU, H., WANG, Q., LI, G. & WAN, L. 2012. Characterization of multi-type mineralizations in the Wandongshan gold poly-metallic deposit, Yunnan (China), by fractal analysis. *Journal of Geochemical Exploration*, **122**, 20–33.
- MANDELBROT, B.B. 1982. *The Fractal Geometry of Nature*. W.H. Freeman, New York.
- MCCUAIG, C.T. & HRONSKY, J.M.A. 2014. The mineral system concept: the key to exploration targeting. *Society of Economic Geologists*, 153–175.
- MCLELLAN, J.G., BLENKINSOP, T.G., NUGUS, M. & ERICKSON, M. 2007. Numerical simulations of deformation and controls on mineralization at the Sunrise Dam Gold Mine, Western Australia. In: ANDREW, C.J. ET AL. (eds) 9th Biennial SGA Meeting, 2007, Association for Economic Geology, Dublin, 1455–1458.
- MILLER, J.McL. & NUGUS, M. 2006. *The structural evolution of the Sunrise Shear Zone and the overlying Watu and Western Shear Zones, Sunrise Dam gold deposit, Laverton, W.A.* Project Y4, pmdCRC.
- MUELLER, A. 2002. A review of U-Pb monazite/xenotime geochronology: implications for the precise age of the Sunrise Dam-Cleo, Wallaby, and other Archean gold deposits in Western Australia. Placer Dome Asia Pacific, internal report.
- OCCHIPINTI, S.A., METELKA, V. ET AL. 2016. Multicommodity mineral systems analysis highlighting mineral prospectivity in the Halls Creek Orogen. *Ore Geology Reviews*, **72**, 86–113.
- ORD, A., HOBBS, B.E. & LESTER, D.R. 2012. The mechanics of hydrothermal systems: I. Ore systems as chemical reactors. *Ore Geology Reviews*, **49**, 1–44.
- ORD, A., MUNRO, M. & HOBBS, B.E. 2016. Hydrothermal mineralising systems as chemical reactors. *Ore Geology Reviews*, **79**, 155–179.
- POUR, A.B., HASHIM, M. & VAN GENDEREN, J. 2013. Detection of hydrothermal alteration zones in a tropical region using satellite remote sensing data: Bau goldfield, Sarawak, Malaysia. *Ore Geology Reviews*, **54**, 181–196.
- RAMANAIDOU, E., WELLS, M., LAU, I. & LAUKAMP, C. 2015. Characterization of iron ore by visible and infrared reflectance and Raman spectroscopies. In: LU, L. (ed.) *Iron Ore – Mineralogy, Processing and Environmental Sustainability*, Woodhead Publishing, Cambridge, 191–228, <https://doi.org/10.1016/B978-1-78242-156-6.00006-X>
- ROACHE, T.J., WALSHE, J.L. & HUNTINGTON, J.F. 2010. *On-Site Validation and Implementation of New Hylogging Technologies – Technology Transfer and Re-Skilling*. Minerals and Energy Research Institute of Western Australia, final project report M400.

- SALAT, H., MURCIO, R. & ARCAUTE, E. 2017. Multifractal methodology. *Physica A*, **473**, 467–487.
- SANISLAV, I.V., BRAYSHAW, M., KOLLING, S.L., DIRKS, P.H.G.M., COOK, Y.A. & BLENKINSOP, T.G. 2016. The structural history and mineralization controls of the world-class Geita Hill gold deposit, Geita Greenstone Belt, Tanzania. *Mineralium Deposita*, **52**, 257–279.
- SCHROEDER, M. 1991. *Fractals, Chaos, Power Laws*. W.H. Freeman, New York.
- SORNETTE, D. 2006. *Critical Phenomena in Natural Sciences; Chaos, Fractals, Self-Organization and Disorder: Concepts and Tools*. Springer, Berlin.
- SPROTT, J.C. 2003. *Chaos and Time-Series Analysis*. Oxford University Press, Oxford.
- SUN, T. & LIU, L. 2014. Delineating the complexity of Cu–Mo mineralization in a porphyry intrusion by computational and fractal modeling: a case study of the Chehugou deposit in the Chifeng district, Inner Mongolia, China. *Journal of Geochemical Exploration*, **144**, 128–143.
- TAPPERT, M., RIVARD, B., GILES, D., TAPPERT, R. & MAUGER, A. 2013. The mineral chemistry, near-infrared, and mid-infrared reflectance spectroscopy of phengite from the Olympic Dam IOCG deposit, South Australia. *Ore Geology Reviews*, **53**, 26–38.
- TURCOTTE, D.L. 1986. A fractal approach to the relationship between ore grade and tonnage. *Economic Geology*, **81**, 1528–1532.
- VEARNCOMBE, J. & ZELIC, M. 2015. Structural paradigms for gold: do they help us find and mine? *Applied Earth Science*, **124**, 2–19, <https://doi.org/10.1179/1743275815Y.0000000003>
- WANG, Q., DENG, J., LIU, H., YANG, L., WAN, L. & ZHANG, R. 2010. Fractal models for ore reserve estimation. *Ore Geology Reviews*, **37**, 2–14.
- WANG, G., CARRANZA, E.J.M. ET AL. 2012. Mapping of district-scale potential targets using fractal models. *Journal of Geochemical Exploration*, **122**, 34–46.
- WANG, R., CUDAHY, T. ET AL. 2017. White mica as a hyperspectral tool in exploration for the Sunrise Dam and Kanowna Belle Gold deposits, Western Australia. *Economic Geology*, **112**, 1153–1176.
- WYBORN, L.A.I., HEINRICH, C.A. & JAQUES, A.L. 1994. Australian Proterozoic mineral systems: essential ingredients and mappable criteria. In: *Proceedings of the Australian Institute of Mining and Metallurgy Annual Conference*, Perth, 109–115.
- WYMAN, D.A., CASSIDY, K.F. & HOLLINGS, P. 2016. Orogenic gold and the mineral systems approach: resolving fact, fiction and fantasy. *Ore Geology Reviews*, **78**, 332–335.
- YARDLEY, B.W.D. & CLEVERLEY, J.S. 2015. The role of metamorphic fluids in the formation of ore deposits. In: JENKIN, G.R.T., LUSTY, P.A.J., McDONALD, I., SMITH, M.P., BOYCE, A.J. & WILKINSON, J.J. (eds) *Ore Deposits in an Evolving Earth*. Geological Society, London, Special Publications, **393**, 117–134. <https://doi.org/10.1144/SP393.5>
- YUAN, F., LI, X. ET AL. 2015. Multifractal modelling-based mapping and identification of geochemical anomalies associated with Cu and Au mineralisation in the NW Junggar area of northern Xinjiang Province, China. *Journal of Geochemical Exploration*, **154**, 252–264.
- ZADEH, M.H., TANGESTANI, M.H., VELASCO ROLDAN, F. & YUSTA, I. 2014. Spectral characteristics of minerals in alteration zones associated with porphyry copper deposits in the middle part of Kerman copper belt, SE Iran. *Ore Geology Reviews*, **62**, 191–198.